Acta Neuropathologica Communications

RESEARCH

Open Access

Spontaneous generation of diverse recombinant prion strains: sulfated glycan cofactors facilitate strain emergence but do not determine specific strain properties

Nuria L. Lorenzo[1†], Hasier Eraña[2,3,4†], Enric Vidal[5,6], Jorge M. Charco[2,3,4], Lucía Parga[1], Carlos M. Díaz-Domínguez[2], Sonia Veiga[1], Susana Bravo[7], Samanta Giler[5,6], Mariví Geijo[8], Jesús R. Requena[1*] and Joaquín Castilla[2,3,9*]

Abstract

Significant advances over the last two decades in the study of in vitro prion formation and propagation have revealed that distinct cofactors can facilitate or induce spontaneous prion misfolding. This, in turn, has raised important questions about the role of cofactors and their potential significance in vivo in prion diseases. Key questions include whether cofactors are necessary for prion infectivity or whether they might play a crucial role in determining strain features without being essential for infection. Grounded in previous work that showed that polyanions such as RNA or dextran sulfate facilitate spontaneous prion misfolding in vitro, we have addressed whether other chemically similar cofactors could expand the diversity of PrP^{Sc} conformers and whether these would exhibit distinctive strain features. Using the Protein Misfolding Shaking Amplification (PMSA) and three different polyanionic cofactors (heparin, chondroitin sulfate and pentosan polysulfate), we obtained and characterized a total of nine conformers and compared them to previously generated strains obtained with dextran sulfate. All nine conformers proved infectious in transgenic mice, generating distinct prion strains and suggesting that different cofactors can indeed drive the formation of distinct conformers. However, the observed variations within conformers generated with the same cofactor indicate a degree of structural flexibility, likely resulting in related but distinguishable groups of conformers. Our study demonstrates that sulfated glycans not only facilitate in vitro spontaneous PrP^{Sc} generation but also enable the emergence of multiple distinct prion strains, providing insights into the molecular mechanisms underlying strain diversity and their potential relevance to spontaneous prion diseases.

Keywords Prion diseases, PrP^{Sc}, Recombinant prions, Cofactors, Spontaneous misfolding, Spontaneous prions, Prion strains, PMSA, Sulfated glycans, Strain diversity

†Nuria L. Lorenzo and Hasier Eraña have same contribution.

*Correspondence:
Jesús R. Requena
jesus.requena@usc.es
Joaquín Castilla
jcastilla@cicbiogune.es

Full list of author information is available at the end of the article

Introduction

Transmissible spongiform encephalopathies (TSE) or prion diseases are a group of rare, fatal, and rapidly progressing neurodegenerative disorders that affect humans and other mammals. According to their etiology, prion diseases can be classified as acquired, genetic or idiopathic conditions (commonly referred to, as sporadic). Acquired cases are related to exogenous exposure to contaminated food, drugs or surgical material; genetic cases are associated with mutations in the prion protein (PrP) gene, and idiopathic prion diseases have no known cause [1, 2]. Idiopathic prion diseases, and specifically, sporadic Creutzfeldt-Jakob disease (sCJD), represent the most common cause of these disorders with 85–90% of diagnosed TSE cases [1, 2], and therefore, understanding the mechanism of spontaneous generation of PrP^{Sc} is of key relevance in the prion field.

Independently of their origin, all prion diseases share a common physiopathological mechanism based on the accumulation of the aberrantly folded form of the cellular prion protein (PrP^{C}), termed PrP^{Sc}, in the central nervous system (CNS) and in lymphoreticular tissues [2–4]. While PrP^{C} is a monomeric, protease-sensitive and globular membrane-anchored glycoprotein, PrP^{Sc} is an insoluble, protease-resistant and β sheet-rich amyloid [1, 2]. The key feature of PrP^{Sc} is that it induces its abnormal conformation to the physiological counterpart through a self-templating process [5]. Although this templating mechanism, leading to propagation of the PrP^{Sc} conformation, is not known at an atomistic level, a general understanding of it has been possible after the groundbreaking cryo-EM-based elucidation of the structure of PrP^{Sc} [6–10]. PrP^{Sc} comprises a Parallel-In-Register-Beta Stack (PIRIBS), spanning PrP residues ~90–230 (mouse numbering) with an intrinsically disordered ~23–90 N-terminal tail. This tail is dispensable for the templating/infectious activity of PrP^{Sc}, which resides in the PIRIBS core [11]. PrP^{C}, in turn, also comprises two domains: an intrinsically flexible/unfolded N-terminal domain that is longer than that of PrP^{Sc}, spanning residues ~23–120, and an α helix-rich globular domain spanning ~121–230 [12, 13]. The ~90–121 flexible/unfolded stretch present in PrP^{C} but not in PrP^{Sc} is very likely key in the templated conversion process given that it can easily dock and lock into the rigid, template-like corresponding isosequential stretch in the surface of PrP^{Sc}. Such spontaneous dock and lock mechanism is typical of seeded templated conversion, and propagation, of amyloid forming proteins that are intrinsically disordered such as Amyloid β [14, 15]. Conversion of the ~90–120 stretch to the PIRIBS conformation is highly favored by the large decrease of enthalpy afforded by the extensive of newly formed cross-β hydrogen bonds, substantially higher than the decrease of entropy incurred in by transition from disorder to a highly ordered β sheet-rich conformation [14, 15]. It is well known, since the seminal studies by Dobson and collaborators, that the amyloid conformation is the most stable one for any protein, as long as the energy barrier to unfold it is provided [16]. Once the ~90–120 stretch is locked in place, the remaining ~121–230 folded domain of PrP^{C} must unfold to dock and lock. The specific atomistic pathway of this part of the conversion remains to be resolved and likely exhibits some characteristics of a polymer-templated conversion as proposed by Griffith in his seminal paper suggesting a proteinic nature for the scrapie agent [17, 18].

But how is the initial PrP^{Sc} assembly formed in spontaneous prion diseases, in the absence of any pre-existing PrP^{Sc} template? How are PrP^{Sc} prions "born"?

To address this question, in vitro models of spontaneous PrP^{Sc} generation are essential. While early experiments showed that small titers of infectivity can be generated by spontaneous conversion of unfolded PrP to an amyloid conformation under denaturing conditions [19], such PrP amyloid conformer is different from *bona fide* PrP^{Sc}, as revealed by atomistic structures resolved by cryo-EM of one type of PrP amyloid [20, 21], and the other [6–10]. Following the groundbreaking generation in vitro of the first *bona fide* PrP^{Sc} from a set of completely defined components including brain-purified PrP^{C} [22], the first spontaneous generation of *bona fide* recombinant PrP^{Sc} was achieved by Wang et al.. using Protein Misfolding Cyclic Amplification (PMCA) adapted to a recombinant PrP^{C} substrate [23]. In the absence of any seed, but in the presence of RNA isolated from normal mouse liver and the anionic phospholipid 1-palmitoyl-2-oleoylphosphatidylglycerol (POPG) as cofactors, these researchers generated a PrP conformer with a 100% attack rate to wild-type mice and a ~90–230 PK-resistant core. In the absence of definitive cryo-EM evidence showing that such conformer is PrP^{Sc}, all the available biological and biochemical evidence suggests that it is. Subsequent studies identified other cofactors such as phosphatidylethanolamine [24–26] as alternative facilitators of spontaneous acquisition of the PrP^{Sc} conformation by recombinant PrP^{C}. Of note, all these cofactors have in common that they are negatively charged/zwitterionic.

The introduction of Protein Misfolding Shaking Amplification (PMSA) [27] represented a substantial leap forward in the modelling of spontaneous generation of PrP^{Sc} *in vitro.* PMSA was originally developed as a robust alternative to PMCA to propagate recombinant PrP^{Sc} using a pre-formed PrP^{Sc} seed, dextran sulfate as cofactor, recombinant PrP^{C} as substrate and shaking in the presence of small zirconia beads as the force to fragment growing recombinant PrP^{Sc} assemblies and thus multiply the templating surfaces [27]. Its efficiency and

scalability allow facile production of milligram quantities of fully infectious recombinant PrP^{Sc}. Furthermore, the use of dextran sulfate results in selection and reproducible propagation of only certain conformers/strains of the several that might be present in the initial seed [28], so that the final PrP^{Sc} product is homogeneous, with biochemical and biophysical properties corresponding to a single strain [27]. Shortly thereafter, the detection of infrequent, random occurrence of spontaneous recombinant PrP^{Sc} species in unseeded samples subjected to PMSA prompted a systematical search for conditions enhancing such events. We found that substitution of zirconia beads by glass beads, and some other minor adjustments led to a robust, reproducible PMSA variant capable of inducing facile, spontaneous generation of recombinant PrP^{Sc} in the absence of a pre-formed PrP^{Sc} seed [29]. Such modified PMSA method easily generates large quantities of spontaneous recombinant PrP^{Sc} in a short period of time, needing just 1–4 passages vs. 17 in the original PMCA-based method [23]. When recombinant bank vole (BV) PrP^{C} with the 109I polymorphism was subjected to this version of PMSA, with dextran sulfate as the sole cofactor, four different conformers/strains of spontaneously generated recombinant $BVPrP^{Sc}$ were obtained, each one with different biochemical and biological properties. These four strains propagated true over many seeded passages [29]. Each strain presented a unique pattern of PK-resistant peptides, incubation time in first and second passages and lesion profile when inoculated to transgenic mice expressing ~ 1x BVPrP(109I) [29]. Subsequently, we applied this methodology to a very large collection of recombinant PrP^{C} substrates from hundreds of species across most mammalian orders and families and achieved spontaneous recombinant PrP^{Sc} from the majority of them [30]. This study demonstrated the versatility of the PMSA method and the many possibilities it offers for the study of spontaneous generation of PrP^{Sc} at the molecular level. For example, given the easiness with which the combination of BVPrP(109I), the most spontaneously prionogenic PrP sequence that we have encountered (further details on its misfolding proneness can be found at the PrPdex webpage, previously published in Eraña et al., 2024 [30]), we wondered whether dextran sulfate was an essential ingredient for such easy conversion into a variety of $BVPrP^{Sc}$ strains, forming a lucky combination with $BVPrP^{C}$, or whether it could be substituted by other polyanionic glycans acting as cofactors. Furthermore, we became interested in knowing whether different cofactors might induce spontaneous PrP^{Sc} conformers with similar biochemical and biological characteristics, so as to begin to tackle the role of cofactors in determining the structure of different PrP^{Sc} strains and its underlying rules.

In this study, we systematically explore how three different negatively charged polysaccharides—heparin, chondroitin sulfate, and pentosan polysulfate—influence spontaneous recombinant PrP^{Sc} generation and conformational diversity. Through biochemical characterization, electron microscopy, and in vivo assessment of infectivity and strain properties, we demonstrate that these different cofactors can generate unique PrP^{Sc} conformers with distinct biological features.

Materials and methods

Expression and purification of Recombinant bank vole PrP 109I

Recombinant full-length bank vole PrP (109I) was expressed in *E. coli* Rosetta (DE3) competent cells (Millipore) harboring the pOPIN E expression vector as previously described [31]. Briefly, the wild-type I109 bank vole *Prnp* sequence (amino acids 23–231, based on GenBank accession number PQ327920) was cloned into the pOPIN E expression vector by homologous recombination after using the oligonucleotides 5' AGGAGATATACCATGAAGAAGCGGCCAAAGCCTGG3' and 5' GTGATGGTGATGTTTGGAACTTCTCCCTTCGTAGTA3' to amplify it from bank vole genomic DNA. Bacteria were transformed by heat-shock and grown in LB broth with 50 µg/mL ampicillin sodium salt at 37 °C with shaking. Protein expression was induced by adding 1 mM Isopropyl β-D-1-thiogalactopyranoside. Subsequently, the bacterial culture was centrifuged at 4,500 *g* for 15 min at 4 °C. Pellets were resuspended and lysed with lysis buffer containing 50 mM Tris-HCl, 5 mM EDTA, 1% Titon X-100, 1 mM PMSF (adjusted to pH 8), 100 µg/mL lysozyme, 100 U/mL DNase, and 20 mM $MgCl_2$. The suspension was then incubated for 30 min with vigorous shaking at room temperature and subsequently centrifuged at 8,500 *g* at 4 °C for 1 h. Pellets containing bacterial inclusion bodies were resuspended in 50 mL of washing buffer (20 mM Tris-HCl, 150 mM NaCl, 1 mM EDTA, 1% Srkosyl, pH 8), and after additional centrifugation at 8,500 *g*, at 4 °C for 1 h, the pellet was dissolved in inclusion buffer containing 20 mM Tris-HCl, 0.5 M NaCl, and 6 M GdnHCl (pH 8). The suspension was incubated overnight at 37 °C with vigorous shaking, followed by final centrifugation at 8500 *g* and 4 °C for 1 h. The supernatant was filtered through a 0.20 µm-pore syringe filter. Protein purification was carried out using a histidine affinity column (HisTrap FF Crude 5 mL chromatographic columns, GE Healthcare) coupled to an ÄKTA Start FPLC system (GE Healthcare). Although this protein does not contain a His-tag, purification was performed with a histidine affinity column, taking advantage of the natural histidine residues present in the octapeptide repeat region of PrP. After purification, the proteins were eluted in 30 mL of elution buffer containing 20 mM Tris-HCl, 500 mM NaCl, 500

mM imidazole, and 2 M GdnHCl (pH 8). Subsequently, the quality and purity of protein batches were assessed by total protein staining after SDS-PAGE. Finally, GdnHCl was added to a final concentration of 6 M. The final protein concentration was adjusted to 25 mg/mL by concentrating using 10 kDa centrifugal filter units (Amicon Ultra-15, 10 kDa, Millipore). For long-term storage, purified protein preparations were aliquoted and frozen stored at – 80 °C.

De novo generation of PrPSc by PMSA with different cofactors

Aliquots of recombinant protein stored at – 80 °C in 6 M GdnHCl were thawed on ice, diluted 1:5 in PBS, and dialyzed against PBS (1:10,000) for 1 h at room temperature. After dialysis, the protein was centrifuged for 15 min at 19,000 *g* and 4 °C. Subsequently, the supernatant containing PrP folded into its native conformation was diluted to a final concentration of 2 µM with conversion buffer (CB) consisting of 0.15 M NaCl and 1% Triton-X-100 in PBS, supplemented with a cofactor: 0.1% (w/v) heparin sodium salt from porcine intestinal mucosa (Sigma, Cat No SRE00027, 15–19 kDa), 0.1% (w/v) chondroitin sulfate sodium salt from shark cartilage (Sigma, Cat No C4384, 50–80 kDa), or 0.1% (w/v) pentosan polysulfate (MedChem Express, 4–6 kDa). Note that heparin and chondroitin sulfate are chemically heterogeneous biopolymers with molecular weights that vary depending on sulfation degree and chain length, resulting in considerable batch-to-batch variability. The mixture containing CB, the recombinant protein, and the corresponding cofactor is referred to hereafter as "substrate". PrP conversion was performed by PMSA as previously described [27]. Briefly, 500 µL of substrate was aliquoted into 2 mL screw-cap conical tubes containing ~ 180 mg of 1 mm or 0.1 mm glass beads (Sigma-Aldrich). Tubes were continuously shaken at 700 rpm at 39 °C for 24 h using thermoblocks (Digital Shaking Drybath, Thermo Scientific). To perform serial rounds of PMSA, a 1:10 dilution of the PMSA product was used as a seed and added to tubes containing fresh substrate supplemented during the first three passages with 0.1–1 mm glass beads, or with 1 mm zirconia-silica beads (BioSpec Products Inc.) for subsequent passages for stabilization. Some of the samples showing spontaneous rec-PrP^{res} after the three serial rounds in the presence of glass beads, chosen for their differences in electrophoretic mobility patterns, were propagated further for stabilization, performing four additional serial PMSA rounds of 24 h with 1:10 dilution. These stabilized PMSA products were used for most biochemical and biological characterization experiments, and also for long-term storage and further propagation through coating of 2.3 mm diameter zirconia-silica beads (BioSpec Products Inc.), as previously explained [32].

Detection of PK-resistant recombinant PrP by total protein staining

The PMSA product was analyzed by SDS-PAGE and stained after digestion with PK. For this purpose, the PMSA product was subjected to PK (Roche) digestion to a final concentration of 25 µg/mL at 42 °C for 1 h. Subsequently, samples were centrifuged at 19,000 *g* at 4 °C for 15 min. The supernatant was carefully discarded, and the pellet was washed with 500 µL of PBS and centrifuged again at 19,000 *g* at 4 °C for 5 min. After removing the PBS, the pellet was resuspended in 15 µL of 1x loading buffer (NuPAGE 4x, Invitrogen Life Technologies) and boiled at 100 °C for 10 min. Subsequently, samples were loaded onto 4–12% acrylamide gels (NuPAGE Midi gel, Invitrogen Life Technologies). Electrophoresis was performed for 1 h 20 min (10 min at 70 V, 10 min at 110 V, and 1 h at 150 V). The gel was then stained using BlueSafe (NZYtech) for total protein staining at room temperature with gentle agitation.

Animal housing and experimental procedures

All animal experiments were conducted in accordance with European and national regulations on animal protection for experimental and other scientific purposes, and with approval from the respective institutional ethics committees.

We used a transgenic mouse model expressing ~ 1x bank vole PrP, bearing isoleucine at position 109 (GenBank accession number PQ327920), hereinafter TgVole(I109)1x (FVB/N.129Ola-Tg (Prnp-Bvole109I) C594PRC/Cicb) [27, 29, 32]. Animals were housed in groups of 3–6 per cage in a controlled environment at a room temperature of 22 °C, with a 12-hour light/darkness cycle, and 60% relativ humidity in HEPA-filtered, individually ventilated cages. Animals had access to food and water *ad libitum*, and received environmental enrichment. For prion transmission experiments, the following protocols were employed.

Inoculum preparation: Inocula from PMSA products were prepared by diluting the PMSA product 1:10 in PBS prior to inoculation. All PMSA-derived inocula were normalized based on equal volumes from reactions containing identical starting amounts of recombinant PrP^{C} substrate, with reactions carried out to conversion plateau where available substrate was depleted. This approach was chosen over quantification of PK-resistant material to avoid potential artifacts from strain-specific differences in protease sensitivity. While this ensures comparable amounts of converted protein across preparations, modest differences in final yields between strains may still influence infectivity comparisons. Similarly, inocula from brain homogenates of terminally ill mice were prepared by diluting to 1% (w/v) in PBS. *Intracerebral inoculation:* Six- to eight-week-old male and female

TgVole(I109)1x mice were anesthetized using either isoflurane (IsoVet, Braun) or a combination of ketamine/medetomidine (75/1 mg/kg) (Imalgene 1000, Boehringer Ingelheim/Domtor, Ecuphar). For the ketamine/medetomidine protocol, anesthesia was subsequently reversed with atipamezole hydrochloride (1 mg/kg) (Antisedan, Ecuphar). Following cranial exposure, a small perforation was created in the right parietal bone, through which 20 µL of inoculum was administered to the right cerebral hemisphere at approximately 3 mm depth using a precision syringe with a sterile 27-gauge hypodermic needle (Terumo). To prevent reflux along the injection tract, the needle remained in position for an additional 20 seconds before gradual withdrawal. Post-procedure, animals received subcutaneous buprenorphine (0.3 mg/kg) for analgesia and were maintained on a heating pad until complete recovery from anesthesia.

Clinical monitoring post-inoculation: Following inoculation, mice were monitored daily for general health status. Detailed clinical assessment was performed twice weekly until the first appearance of neurological signs, after which monitoring was increased to daily observation. The presence of TSE-associated clinical signs was scored (0–3) based on the following parameters: kyphosis, gait abnormalities, altered coat state, depressed mental state, flattened back, eye discharge, hyperactivity, loss of body condition, and incontinence. Animals showing sustained clinical signs (score ≥ 2 in two or more categories) or severe neurological impairment that compromised welfare were humanely euthanized by cervical dislocation and subsequent decapitation. Survival time was calculated as the interval between inoculation and euthanasia, expressed as days post-inoculation (dpi). Attack rate was determined as the ratio between animals developing confirmed prion disease (by histopathological and/or biochemical analyses) and the total number of inoculated animals. Animals found dead due to intercurrent disease before 100 days post-inoculation were excluded from the study. Results are expressed as mean incubation period ± standard error of the mean (SEM) for each experimental group. Brains were removed and cut sagittally into two halves. One half was frozen for biochemical characterization, and the other half was fixed in 4% paraformaldehyde (PFA) in PBS for histopathological and immunohistochemical analysis.

Histopathological and immunohistochemical analysis

For histopathological analyses, transverse sections of the fixed brains were performed at the levels of the medulla oblongata, piriform cortex, and optic chiasm (Supplementary Fig. 1). Samples were embedded in paraffin wax after dehydration through increasing alcohol concentrations and xylene. For morphological evaluation, 4 µm sections were mounted on glass microscope slides and stained with hematoxylin (Sigma-Aldrich) and eosin (Casa Álvarez). For immunohistochemical analysis, sections were mounted on 3- triethoxysilylpropylamine-coated glass microscope slides (DAKO). Deparaffinized sections were subjected to epitope retrieval by immersion in formic acid and boiling at low pH (6.15) in a pressure cooker, followed by pre-treatment with proteinase K (Roche). Endogenous peroxidases were blocked by immersion in 3% H_2O_2 in methanol. Subsequently, sections were incubated overnight with anti-PrP 6C2 monoclonal antibody (1:1000) (CVI-Wageningen UR) and visualized using the goat anti-mouse EnVision system (DAKO) with 3,3'-diaminobenzidine (Sigma-Aldrich) as the chromogen substrate. For negative controls, incubation with the primary antibody was omitted.

Spongiform lesion was evaluated following a semiquantitative approach previously described [33]. Briefly, fourteen different brain areas were examined (Supplementary Fig. 1): piriform cortex (Pfc), hippocampus (H), occipital cortex (Oc), temporal cortex (Tc), parietal cortex (Pc), frontal cortex (Fc), striatum (S), thalamus (T), hypothalamus (HT), mesencephalon (M), medulla oblongata (Mobl), cerebellar nuclei (Cm), cerebellar vermis (Cv), and cerebellar cortex (Cc). Spongiform lesions in each area were scored as follows: (0) absence of spongiosis, (1) mild, (2) moderate, (3) intense, and (4) maximum level of lesion. Each area was evaluated globally as a region for scoring. Brain lesion profiles were plotted using the anatomical regions and the mean of the semiquantitative spongiosis scores for each area. Error bars represent the standard error of the mean [33].

Western blot of brain homogenates

Frozen brains were suspended at 10% (w/v) in PBS containing complete protease inhibitors cocktail (Roche) and were homogenized using a Dounce homogenizer until a homogeneous mixture was obtained. Brain homogenates were stored at – 80 °C. Fifteen microliters of brain homogenates was mixed with 5 µL of buffer containing 2% (v/v) NP40 and 5% (w/v) Sarkosyl in PBS, or alternatively, 10 µL of brain homogenate was mixed with 10 µL of the same digestion buffer. Subsequently, samples were digested with 85 µg/mL PK for 1 h at 56 °C and 450 rpm. The reaction was stopped by adding loading buffer (1:3 ratio) and heating at 99 °C for 10 min. For PNGase F digestion, the same 10% brain homogenates were digested with PK as indicated above and immediately after digestion, denaturing buffer [20% SDS (NZYTech) and 100 mM of DTT (Sigma-Aldrich)] was added to each sample for a final concentration of 4% SDS and 20 mM of DTT. The samples were incubated at 100 °C for 30 min and then precipitated with ice-cold methanol, by incubating the samples at – 20 °C for 30 min and centrifugation at 20,000 *g* for another 30 min. Supernatants were

discarded, and the pellets were air-dried prior to PNGase digestion. Dry pellets were resuspended in 1X PNGase F buffer and digested with 1.5 µl of PNGase F (Gibco) for 1 h at 50 °C. Digestion was stopped by adding NuPage 4X Loading Buffer (Invitrogen Life Technologies) and boiling them for 10 min. Samples were electrophoresed on 4–12% acrylamide gel (NuPAGE Midi gel, Invitrogen Life Technologies) and transferred to a PVDF membrane using the iBlot 3 (Invitrogen Life Technologies) transfer system. Subsequently, blocking, washing, and antibody incubations were performed with the iBind™ Flex Western Device (Invitrogen Life Technologies). The primary monoclonal antibody used was SAF83 (1:400) (recognizing epitope 130–160) (Vitro S.A.), and the secondary antibody was peroxidase-conjugated anti-mouse IgG (m-IgGκ BP-HRP, Santa Cruz Biotechnology). Images were acquired using the iBright CL750 imaging system (Invitrogen Life Technologies). Glycoform ratio quantification was performed over digitalized WB images through densitometric analysis, done using the AlphView software (Version 3.4.0, FluorChem Q).

Mass spectrometry

For mass spectrometry-based analysis, 2 mL of the PMSA product was digested by adding PK to a final concentration of 25 µg/mL and incubating at 42 °C for 1 h. After digestion, samples were centrifuged for 30 min at 19,000 *g*, the supernatant was discarded, and the pellet was resuspended and washed with 1mL of PBS. Subsequently, the sample was centrifuged again for 30 min at 19,000 *g*, the supernatant was discarded, and the pellet was resuspended in 50 µL of 6 M GdnHCl with 3 pulses of a tip sonicator and incubated for 1 h at 37 °C. After incubation, TFA was added to a final concentration of 1%. Samples (4 µL) were injected into a nanoLC 400 micro liquid chromatography system coupled to a Triple TOF 6600 high-speed mass spectrometer with a microflow source (SCIEX) and equipped with a silica-based reversed-phase ChromXP C18 column (150 × 0.30 mm, 3 µm particle size, 120 Å pore size). A YMC-TRIART C18 trap column was connected online prior to the separating column (3 µm particle size, 120 Å pore size) (Tecnokroma). After sample loading and washing with 0.1% formic acid in water to remove GdnHCl and other non-peptide components, the flow was switched to the analytical column, and separation proceeded at a flow rate of 5 µl/min with a solvent system consisting of 0.1% formic acid in water as mobile phase A, and 0.1% formic acid in acetonitrile as mobile phase B. Peptides were separated over 40 min with a gradient ranging from 2% to 90% mobile phase B. Data acquisition was performed using a TripleTOF 6600 System (SCIEX) with a data-dependent workflow. Source and interface conditions were as follows: ionspray voltage floating (ISVF) 5500 V, curtain gas (CUR) 25, collision energy (CE) 10, and ion source gas 1 (GS1) 25. The instrument was operated with Analyst TF 1.7.1 software (SCIEX). Switching criteria were set to ions with mass-to-charge ratio (m/z) greater than 350 and less than m/z 1400, with a charge state of 2–5, a mass tolerance 250 ppm, and an abundance threshold of more than 200 counts (cps). Previously targeted ions were excluded for 15 s. The instrument was automatically calibrated every 4 h using tryptic peptides from PepCalMix (SCIEX) as an external calibrant. For data analysis, the sample TIC was analyzed using the PeakView2.2 software, which allows protein reconstruction. The LC-MS Peptide Reconstruct feature uses a peak-finding algorithm to identify groups of peaks that form isotope series and charge series. Protein deconvolution was carried out in the range of 800 to 20,000 Da. PK-resistant fragments were identified using the GPMAW software tool, based on a ± 1 Da difference between the observed peak and the theoretical molecular mass.

Transmission electron microscopy

Zirconia-silica beads coated with each PMSA product were used as seeds to propagate the nine different conformers for their purification and visualization by transmission electron microscopy with negative staining. Using 2–3 prion-loaded beads for each PMSA product, two-step PMSA reactions were performed. First, 4 mL of substrate was seeded and submitted to PMSA for 4 h, which was then transferred to fresh substrate (1:5 dilution) supplemented with clean zirconia-silica beads and subjected to an additional 20 h of PMSA. Sodium dodecyl sulfate (SDS) was added to a final concentration of 0.1% (v/v) to the approximately 20 mL of each PMSA product, which was then incubated at room temperature for 2 h on a rotating mixer. After centrifugation of the PMSA products at 100 *g* in a swinging-bucket rotor for 10 min at RT. Subsequently, most of the supernatant was recovered and centrifuged again at 1,000 *g* for 90 min at RT. In this case, most of the supernatant was discarded and the pellet was resuspended in the remaining volume (approximately 100 µL) and washed with 2 mL of 10 mM Tris-NaCl containing 0.1% of SDS. These concentrated samples were digested with 150 µg/ml of PK at 37 °C for 45 min with mild shaking. After digestion, they were centrifuged at 1000 *g* for 10 min at RT using a swinging-bucket rotor, and the supernatants were completely discarded. The pellets were washed three times using 10 mM TrisNaCl with 0.05% of SDS in the first wash and 10 mM Tris NaCl with 0.02% of SDS in the subsequent washes. After the final wash and centrifugation at 1000 *g* for 5 min at RT, the supernatant was completely discarded and the final pellet for each PMSA product was resuspended in 20–50 µL of 10 mM Tris-NaCl with 0.02% SDS. After thorough resuspension, each sample was deposited onto freshly

glow-discharged carbon-coated copper grids (Carbon Film 400 Mesh, Cu, Electron Microscopy Sciences). After 1 min at RT, the grids were washed with deionized water for 1 min and stained with freshly prepared, filtered 5% uranyl acetate solution for 45 s. Imaging was conducted using a JEM-1230 (JEOL) transmission electron microscope operated at 100 kV and equipped with an Orius SC1000 CCD camera (GATAN).

Quantitative morphological analysis of fibril heterogeneity

To address the morphological diversity observed among different conformers, a systematic quantitative analysis was performed on transmission electron microscopy images. Eighteen representative TEM micrographs were selected for each of the nine conformers (Hep01-03, CoS01-03, PPS01-03) and arranged in 6 × 3 grids for comprehensive visualization (Supplementary Fig. 7. Images were acquired using identical microscopy conditions without pre-selection bias. Fields were captured sequentially as soon as fibrils became visible, with only overlapping fields containing identical structures being excluded. No selection was made based on fibril type, size, or density within each field. All image acquisition and subsequent quantitative analyses were performed by a single observer to ensure consistency.

Preliminary assessment of fibril populations showed that eight conformers presented predominantly uniform morphological characteristics within each image set, whereas CoS02 displayed two morphologically distinct fibril subpopulations that were analyzed separately (CoS02a and CoS02b).

Quantitative morphological classification was performed according to three parameters: Fibril Length (< 50 nm, 50–200 nm, 200–500 nm, > 500 nm), Curvature Measurements (straight, slightly curved, moderately curved, highly curved), and Bundling Frequency (isolated fibrils, small bundles, large bundles). Each parameter was assessed independently of total fibril number per field. To ensure comparability across images with varying fibril densities, raw counts were converted to percentages relative to the total fibril population within each image.

Quantitative data are expressed as mean ± standard error of the mean (SEM) calculated from the 18 individual measurements per conformer. Conformer-specific morphological profiles were generated by averaging percentage values across all analyzed parameters.

Statistical analysis

Statistical analyses were performed using GraphPad Prism 8 (GraphPad Software, San Diego, CA, USA). Descriptive statistics including mean, standard deviation, and standard error of the mean (SEM) were calculated for each experimental group of mice. Incubation periods were expressed as mean ± SEM and compared between groups using one-way ANOVA followed by Games-Howell's multiple comparisons test when appropriate. Survival time was also plotted as Kaplan-Meier survival curves. Attack rates were calculated as the percentage of animals developing confirmed prion disease (determined by clinical signs, histopathology, and/or biochemical analysis) relative to the total number of inoculated animals. For semiquantitative histopathological scoring, lesion profiles were compared between conformers using non-parametric tests (Kruskal-Wallis followed by Dunn's multiple comparisons test) due to the ordinal nature of the scoring system (0–4 scale). Statistical significance was set at $p < 0.05$ for all analyses. Data are presented as mean ± SEM unless otherwise indicated.

Results

Recombinant bank vole (I109) PrP spontaneously misfolded by PMSA exhibits the key biochemical hallmarks of bona fide prions

As a logical next step from our previous work [29, 30] we decided to explore whether dextran sulfate could be replaced by a different polyanionic glycan, with a particular interest in the emergence of more than one PrP^{Sc} strain. We thus substituted dextran sulfate by two glycosaminoglycans (GAGs), heparin and chondroitin sulfate, and one GAG mimic, pentosan polysulfate. We chose them because, while they are different from dextran sulfate, they share with them common features such as high density of negative charges afforded by $-SO_3^-$ moieties (Supplementary Fig. 2). Furthermore, GAGs are physiologically relevant to prion disease progression in vivo as shown before [34]. For our purpose, 6 independent, unseeded PMSA reactions were set up for each of the three cofactors, 3 with 0.1 mm and 3 with 1 mm glass beads (Supplementary Fig. 3). Each reaction was submitted to 3 serial PMSA rounds of 24 h. After each round a portion of the reaction product was added to the next reaction mixture. Another portion of the reaction product was used to assess the presence of PK-resistant PrP, a surrogate of PrP^{Sc} emergence. For this, the sample was subjected to PK treatment (25 µg/mL, 1 h, 42 °C, 1/0.43 molar ratio PrP/PK) and PK-resistant fragments assessed by SDS-PAGE with total protein staining [29, 30]. After three rounds, 3 of the 6 serial reaction products of each cofactor set, showing apparently distinct PK fragmentation patterns were chosen as distinct rec-PrP^{Sc} conformer candidates. We provisionally assumed these products to be PrP^{Sc} based on their PK-resistant pattern being overall similar -if with nuances- to those of previously generated and propagated recombinant prions, and to their in vitro propagative nature. Of note, PK-resistant PrP bands were already found in 15/18 tubes after the first round of PMSA, and in 18/18 after the third round. Thus, the frequency of potential spontaneous misfolding was

83% in the first, 89% i the second and 10% in the third PMSA rond. These results are comparable to those previously obtained with dextran sulfate [29], demonstrating that heparin, chondroitin sulfate and pentosan polysulfate are roughly equipotent to dextran sulfate as facilitators of spontaneous generation of recombinant bank vole PrP^{Sc}. The consistent emergence of PK-resistant products across different cofactors supports the hypothesis that polyanionic molecules share common mechanisms for facilitating spontaneous prion misfolding.

These 9 distinct reaction products, hereafter referred to as "spontaneous rec-PrP^{Sc} conformers", were subsequently propagated using standard PMSA with zirconia beads [27] (Supplementary Fig. 3) and PK-resistant patterns of stabilized products are shown in Fig. 1.

Several conformers obtained with different cofactors appeared to be remarkably similar; for example, PPS02 is very similar to Ust09, and Hep01 to CoS03. However, careful semiquantitative assessment of band intensities showed every conformer to be unique (Supplementary Fig. 4). No obvious cofactor-specific trend could be discerned. Every conformer presented a ~ 16 kDa PK-resistant band, corresponding to the classic ~ 90–231 PrP^{Sc} PK-resistant fragment (bank vole PrP numbering). This fragment, with added mass from glycans and GPI-anchor, is referred to as PrP27-30 in brain-derived PrP^{Sc} [2, 35–37]. This PK-resistant fragment is now known to correspond to the PrP^{Sc} PIRIBS core [6–10] and is also prominent in all *bona fide* rec-PrP^{Sc} generated to date, whether spontaneously or by seeded templating of rec-PrP^{C} [23–25, 27, 29, 30, 37]. In addition to this fragment, the 9 different conformers featured combinations of 4 main additional PK-resistant fragments with apparent molecular masses of ~ 9, ~8, and ~ 6 kDa (Fig. 1). An exact identification of these fragments, carried out by means of mass spectrometry, will be described in the next section. However, we can anticipate that the ~ 9 and ~ 6 kDa bands are C-terminal and N-terminal fragments of the ~ 16 kDa band, respectively, resulting from a secondary PK nick at Asn153 or Met154, whereas the ~ 8 kDa fragment result from an alternative nick at Tyr163. No N-terminal fragment complementary to this fragment was detected. Other minor fragments were seen across the different conformers. Similar patterns have been obtained for other PMSA-derived rec-PrP^{Sc} conformers; their main difference from patterns obtained from brain-derived PrP^{Sc} conformers such as RML, GPI-less RML, 263 K, or Drowsy is the larger abundance of fragments derived from internal nicks in the putative PIRIBS core.

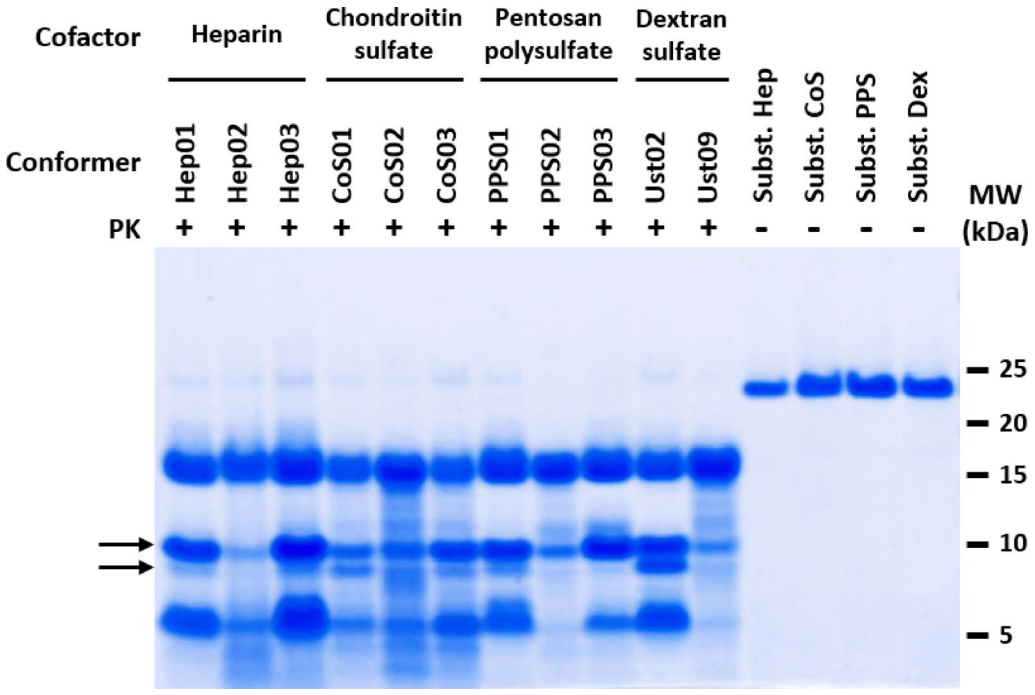

Fig. 1 Distinct electrophoretic mobility patterns following PK digestion of spontaneously misfolded recombinant PrP using PMSA and 3 different polyanionic cofactors. Three PMSA-treated samples with heparin displayed distinct patterns of PK-resistant fragments, with different proportions of specific fragments. For example, Hep02 features a dominant ~16 kDa fragment and much fainter ~9 kDa and ~6 kDa fragments, which are much more intense in Hep01 with respect to the ~16 kDa fragment. In some cases, differences in the patterns are subtle, as observed between Hep01 and Hep03. Similar differences exist between the 3 different patterns observed with chondroitin sulfate and those with pentosan polysulfate. For comparison, patterns from two conformers previously generated with dextran sulfate, Ust02 and Ust09 [29], are also shown. Molecular weight markers slightly overestimate the real MW of PK-resistant PrP fragments (see mass spectrometry-based data below). The arrows indicate ~9 kDa and ~8 kDa fragments, respectively

A

	Fragment	Theoretical mass (Da)	Observed mass (Da)[1]	From conformer[2]	Seen also in conformers[3]
C-terminal fragments	G92-S231[4]	15934.5	15935.3	Hep02	Hep03
	N97-S231	15227.0	15225.1	Cos02	-
	Q98-S231	15411.3	15411.3	Hep01	Hep02, Hep03, CoS02, CoS03
	A133-S231	11992.1	11991.3	CoS03	-
	N153-S231	9436.4	9436.5	Hep01	Hep02, Hep03, CoS02, CoS03
	M154-S231	9322.2	9322.8	Hep03	CoS02
	Y163-S231	8155.9	8155.5	Hep01	Hep02, CoS02, CoS03
N-terminal fragments[5]	N97-Y150	5821.5	5821.9	Hep01	Hep03
	N98-Y150	5707.4	5707.9	Hep01	Hep03, CoS03
	W99-Y150	5579.3	5579.0	Hep03	CoS03
	Q98-N153	6106.9	6106.2	CoS02	-
	N97-R136	3996.6	3996.8	Hep02	Hep03

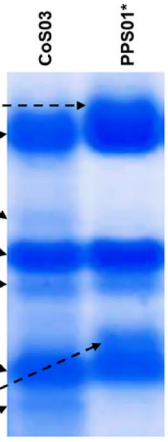

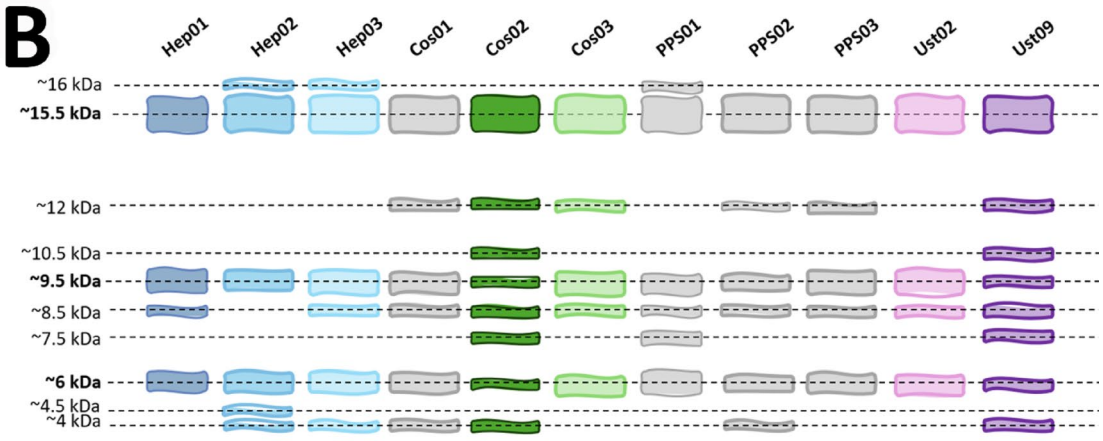

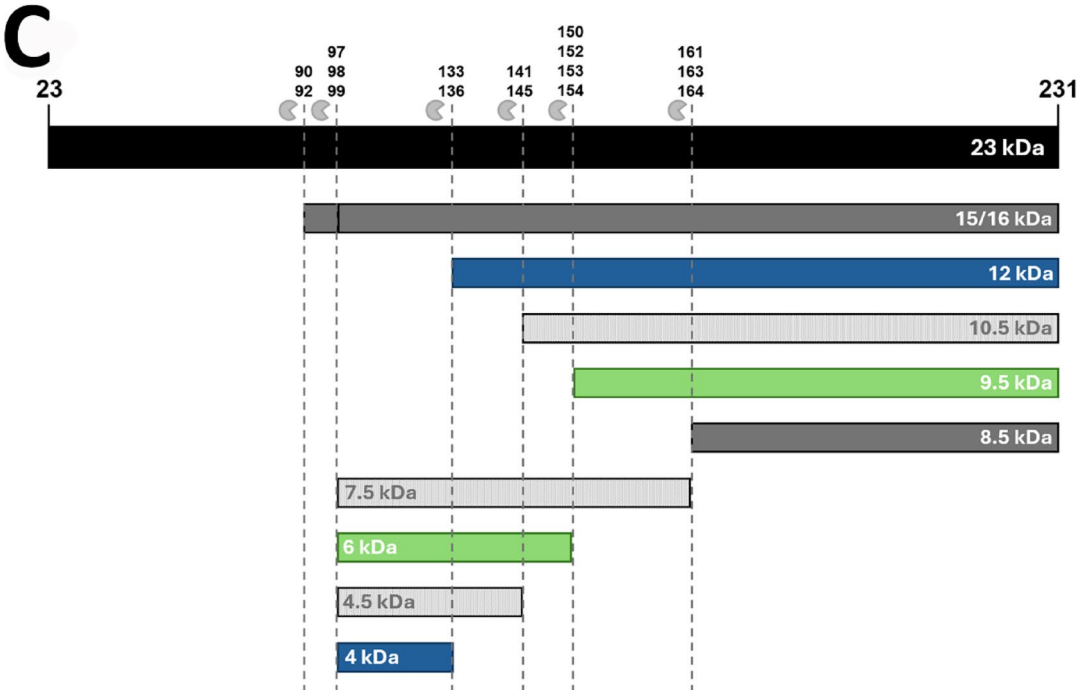

Fig. 2 (See legend on next page.)

(See figure on previous page.)

Fig. 2 Mass spectrometry-based identification of PK-resistant fragments in spontaneous rec-PrP^{Sc} conformers generated with different sulfated glycan cofactors and illustrations of the corresponding fragments. **A** Left: Table listing the masses observed in the spectra for the conformers analyzed by this method, and their correspondence with the exact theoretical masses of possible BVPrP(109I)23–231 fragments. [1]Observed mass in the deconvoluted spectrum; [2]fragments potentially detected in other conformers (within ±1 Da variation) or with +16 Da (methionine oxidation, a modification that can occur during sample manipulation for analysis); [3]conformers where the unmodified fragment was detected. The non-quantitative nature of the mass spectrometric method used (nano HPLC coupled to electrospray) does not preclude that the fragment may have been present in more spectra.[4]Fragments from contiguous or almost contiguous cleavages (PK nick spots) are grouped in the table and complementary N and C-ter fragments (A + B = approximately 92/98–231) are colored in blue and green; [5]N-terminal with respect to the 92/98–231 larger PK-resistant core. Arrows connect the specific, mass spectrometry-identified masses with SDS-PAGE fragments. Right: Total protein, BlueSafe-stained SDS-PAGE gel showing two representative conformers (reproduced from Fig. 1). PPS01 was included although it was not subjected to MS analysis because, together with CoS03, it most clearly displays the main bands detected in the MS-analyzed preparations. **B** Schematic representation of electrophoretic banding patterns for all rec-PrP^{Sc}. All the PK-resistant PrP fragments detected either in total protein staining (Fig. 1) or MS are depicted for each conformer, including Ust02 and Ust09 previously generated with dextran sulfate. Conformer colors correspond to those used in the densitometric analysis (Supplementary Fig. 2). Grey conformers could only be analyzed by electrophoresis and total protein staining. Fragment sizes are indicated on the left, with major fragments detected in all conformers shown in bold. **C** Schematic of N- and C-terminal fragments relative to full-length recombinant bank vole PrP (black bar). Using the color scheme from panel A, complementary C- and N-terminal fragments are colored blue and green, respectively. Dark grey fragments were detectable by both techniques, while light grey fragments were detected by only one technique, likely due to technical limitations such as insufficient Coomassie resolution. Fragment sizes are indicated within each bar, and cleavage sites identified by MS are shown above the full-length rec-PrP sequence

A detailed discussion is presented in the Supplementary Material (Supplementary Fig. 5).

Mass spectrometry reveals distinct protease cleavage patterns specific to each conformer

We next aimed to characterize, with greater accuracy, the PK-resistant fragments present in each PMSA product. For this purpose, we used mass spectrometry (MS). We obtained spectra from the three conformers generated with heparin and two of the conformers generated with chondroitin sulfate, whereas the analysis could not be completed for CoS01 and the three PPS conformers due to technical limitations. Nonetheless, given that all the fragments detectable in the conformers generated spontaneously were represented in the samples that could be analyzed, we extrapolated the results to the equivalent fragments observed by total protein staining in those conformers that could not be analyzed via MS. The most common cleavage sites, present in all analyzed conformers, were N97, Q98, Y150, N153, and M154 (Fig. 2 and Supplementary Figs. 5 and 6), which generated the peptides N97-Y150, Q98-N150, N153-S231, and M154-S231. Additional less frequent cleavage sites —not present in all conformers— were G90, G92, H96, W99, A133, A136, F141, W145, R151, V161, Y163, or R164 (Fig. 3 and Supplementary Fig. 6). Notably, most of these cleavage sites have been previously described in brain-derived and recombinant prion strains: G90, G92, N97, A133, N153, M154, and Y163 (bank vole numbering) [35, 37–41]. This analysis clearly shows that the stable fragmentation pattern of different conformers, reproducible over successive PMSA passages, is unique to each strain. If we assume that a single rec-PrP^{Sc} conformer exists in each PMSA product, these cleavage sites would correspond to regions in its structure that are more accessible to PK and perhaps more flexible. For example, the brain-derived conformer GPI-less RML PrP^{Sc} has its main PK cleavage site at residues 90/92, at the border between the PIRIBS core and its N-terminal flexible tail. After deglycosylation with PNGase F, this conformer generates the classic ~ 20 kDa PK-fragment [11] but also a minor fragment at residues 152/153 and several other, even more minor fragments [35] which are located in the PIRIBS core (Supplementary Fig. 5). An alternative explanation for the fragment pattern would be the coexistence of more than one PrP^{Sc} conformer, but this is unlikely, as it would require an exquisite equilibrium during propagation, such that one does not eventually outcompete others. On the other hand, the coexistence of a minor fraction of alternative conformers, contributing little to the pattern, as posited by the quasi-species hypothesis [42], cannot be ruled out.

Transmission electron microscopy shows morphological diversity correlating with biochemical properties

We used negative-stain transmission electron microscopy (TEM) to assess the general appearance of the 9 different conformers obtained. Figure 3 shows a representative selection of images from five of the conformers. All conformers were fibrillar, displaying ~ 12 nm wide, unbranched fibrils that showed a tendency to associate laterally, forming bundles. Some of the fibrils were clearly twisted, with a half pitch of ~ 200 nm (Fig. 3A), although many fibrils appeared flat (Fig. 3B). The length of the fibrils varies considerably, with many in the 200–500 nm range. However, longer fibrils reaching ~ 1 μM were also observed (Fig. 3B).

A systematic quantitative analysis of fibril morphology across 162 TEM micrographs (18 per conformer) revealed five distinct morphological patterns based on fibril length distribution, curvature characteristics, and bundling behavior (Supplementary Fig. 7; high-resolution images accessible via individual micrograph links).

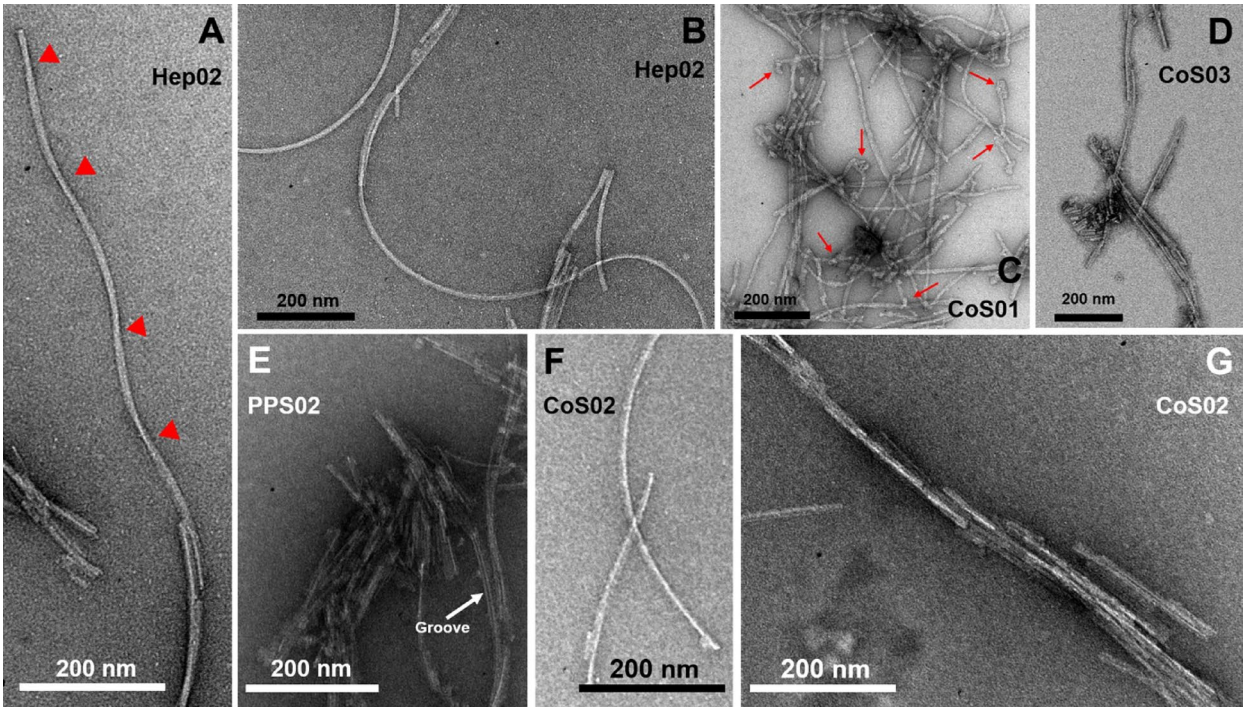

Fig. 3 Gallery of negative-stain TEM images of spontaneous rec-PrP^{Sc} conformers. **A**: Hep02, showing an abundance of long, curved fibrils. Twists with a half pitch of ~ 200 nm are evident in some fibrils. **B**: Extremely curved fibrils in Hep02; the fibril in the upper-left corner appears to be flat for ~ 600 nm. **C**: CoS01, displaying predominantly shorter, straight fibrils. Twists are apparent in some fibrils. Lateral bulges are seen associated with many fibrils; some examples are marked with red arrows. **D**: CoS03, also displaying predominantly shorter, straight fibrils. Note that the PK-resistant pattern of CoS03 is very similar to that of CoS01 (Figs. 1 and 2). **E**: PPS02 with a mixture of curved and short, straight fibrils. A central groove can be seen in two fibrils. **F**: Curved fibrils in CoS02, which are characteristic of this conformer and whose PK-resistant pattern is similar to that of Hep02. **G**: Shorter, straight fibrils in CoS02 of the type also present in other conformers such as Hep02

Morphotype 1 (☯-blue): Characterized by predominance of short-to-medium fibrils (< 50–200 nm, ~ 35–65%), predominantly straight morphology (~ 50–65%), and high frequency of isolated fibrils (~ 35–45%). This pattern was observed in Hep01, Hep03, PPS01, PPS02, and PPS03.

Morphotype 2 (☯-brown): Distinguished by balanced fibril length distribution with notable presence of long fibrils (200–500 nm, ~ 25–35%), mixed curvature profile with increased moderately-to-highly curved fibrils (~ 75%), and low bundling tendency. This morphotype was less prevalent among the analyzed conformers. Observed primarily in CoS01.

Morphotype 3 (Ψ): Defined by predominance of long fibrils (> 500 nm, ~ 40–60%), high curvature index with abundant moderately-to-highly curved fibrils (~ 55%), and tendency toward small bundle formation (~ 50%). Observed primarily in Hep02 and CoS02a.

Morphotype 4 (Ω-blue): Characterized by heterogeneous length distribution with significant representation across all size categories, balanced curvature profile, and diverse bundling patterns including large bundles (~ 15–25%). This pattern showed intermediate characteristics between other morphotypes. Observed primarily in CoS02b.

Morphotype 5 (Ω-brown): Distinguished by unique bimodal distribution with both very short (< 50 nm, ~ 40–50%) and long (200->500 nm, ~ 25%) fibrils, variable curvature characteristics, and strong propensity for bundle formation (~ 65%). Observed in CoS03 with distinctive features.

CoS02 presented a unique case with clearly distinguishable mixed populations (CoS02a and CoS02b), analyzed separately due to the presence of two morphologically distinct fibril types within the same conformer population.

The micrographs used for the quantitative analysis, as well as the raw data and a plot summarizing the quantification of the main characteristics of the fibrils found in each preparation are provided in Supplementary Fig. 7.

All nine conformers are infectious and exhibit distinct strain properties in vivo

Based on the biochemical data, we had generated 9 authentic spontaneous rec-PrP^{Sc} conformers. We therefore sought to evaluate whether they were infectious and possessed distinct biological properties that

would classify them as *bona fide* prion strains. For this, we inoculated each conformer into groups of 5–9 TgVole(I109)1x transgenic mice. This well-characterized transgenic mouse model [27, 32] expresses approximately 1x BVPrP(109I) in an MoPrP-null background. As seen in Table 1; Fig. 4A, all 9 conformers were infectious and generated fatal, neurodegenerative prion diseases with attack rates of 100% in all cases except for CoS01, that showed 60% attack rate with all 5 animals showing neurological signs but PrP^{Sc} being detectable in only three of them. Incubation times ranged from 105 ± 2 to 363 ± 7 days (Hep03 and Hep01, respectively). No obvious correlation between biochemical properties and incubation times was apparent. For example, Hep01 and Hep03 have very similar PK-resistant patterns (Fig. 1, and Supplementary Fig. 4), yet they exhibited the most divergent incubation times. Conversely, Cos02 and PPS02, which display predominantly curved, long fibrils and relatively similar PK-resistant patterns (Figs. 1 and 3, and Supplementary Fig. 4), showed similar incubation times (144 ± 1 and 141 ± 4 days, respectively), but Hep02, despite having similar characteristics, had a substantially longer incubation time (220 ± 13 days). Western blot analysis of brains from euthanized mice showed, in all cases, the presence of PK-resistant PrP with the characteristics typical of classic PrP^{Sc} (Supplementary Fig. 8A). These results confirm that we have generated *bona fide* prion strains with each of the different cofactors used. We then performed a second passage by inoculating TgVole(I109)1x mice with 1% brain homogenates from mice from the first passage. As shown in Table 1; Fig. 4B, incubation times shortened considerably, ranging from 74 ± 2 (CoS03) to 106 ± 2 days (PPS01). No obvious correlation between the incubation time lengths in the first and second passages could be detected. For instance, the incubation time of Hep01 changed from 363 ± 7 to 86 ± 5, that of Hep02 from 220 ± 13 to 84 ± 3, and that of Hep03 from 105 ± 2 to 95 ± 4 days. In other words, from very different values, all three converged to similar ranges, with reductions representing 24%, 38%, and 90% of the initial values, respectively. Notably, the conformer that had the shortest incubation time in the first passage had the longest one in the second passage, at least within the heparin-derived conformer group. Similar patterns were observed for conformers from the other cofactor groups, and for comparisons of incubation time changes across groups. Western blot analysis of brains from these animals showed in all cases the presence of a classical three bands PrP^{res} with similar mobility patterns to those in the first passage for most preparations, although changes in the size of the non-glycosylated PrP^{res} can be hinted in few of them, such as CoS02 and CoS03 (Supplementary Fig. 8B). To further reveal potential differences in electrophoretic mobility patterns of the distinct preparations after primary and secondary transmission into TgVole(I109)1x mice, a glycoform ratio quantification was carried out, showing subtle differences in the proportion of non-, mono- and diglycosylated PrP^{res} between the distinct preparations (Supplementary Fig. 8C). Despite all being predominantly diglycosylated, distinct ratios were evident in first passage for prions obtained in the presence of each cofactor, but also between samples obtained with the same cofactor, except for those prepared in the presence of chondroitin sulfate, presenting similar proportion of glycoforms. In second passage, the prions generated in the presence of heparin seem to converge, although

Table 1 Infectious nature of the spontaneous rec-PrP^{Sc} conformers generated with 3 different GAG cofactors

Cofactor	Conformer	First passage			Second passage		
		Attack rate	Incubation period (dpi ± SEM)	PrP^{Sc} (WB)	Attack rate	Incubation period (dpi ± SEM)	PrP^{Sc} (WB)
Heparin	Hep01	7/7*[1]	363 ± 7	7/7	6/6*[1]	86 ± 5	6/6
	Hep02	6/6	220 ± 13	6/6	6/6	84 ± 3	5/5[#]
	Hep03	5/5*[1]	105 ± 2	5/5	6/6	95 ± 4	6/6
Chondroitin sulfate	CoS01	3/5*[2]	280 ± 32	3/5	6/6	101 ± 3	6/6
	CoS02	7/7	144 ± 1	7/7	6/6*[2]	102 ± 7	6/6
	CoS03	5/5*[1]	111 ± 5	5/5	6/6	74 ± 2	6/6
Pentosan polysulfate	PPS01	6/6*[1]	292 ± 24	6/6	6/6*[4]	106 ± 2	5/5[#]
	PPS02	8/8	141 ± 4	7/7[#]	6/6*[1]	79 ± 2	6/6
	PPS03	7/7	167 ± 3	7/7	6/6*[1]	103 ± 2	6/6
Dextran sulfate	Ust02	9/9	101 ± 4	9/9	7/7	80 ± 3	7/7
	Ust09	7/7	169 ± 5	7/7	5/5	110 ± 2	5/5

PrP^{Sc}: Classic PrP^{Sc} deposition detected in the brain of recipient mouse by Western blotting

Dextran sulfate: Spontaneous rec-PrPSc strains generated in the past with PMSA with dextran sulfate as a cofactor [29]. The asterisk (*) indicates that some animal from those groups died of intercurrent diseases at times below the half of the mean incubation period of the diseased animals; such animals from were excluded from the analysis. The number of such animals is indicated as a superscript next to the asterisk

Hash (#) represents groups with animals whose brains were not possible to extract (e.g., they were found dead), although they presented clinical signs, and for this reason, the attack rate and the brains with PrPSc do not match, but were considered positive in terms of attack rates due to clear signs of neurological impairment and incubation periods compatible with those of other PrPSc-positive animals from the same group

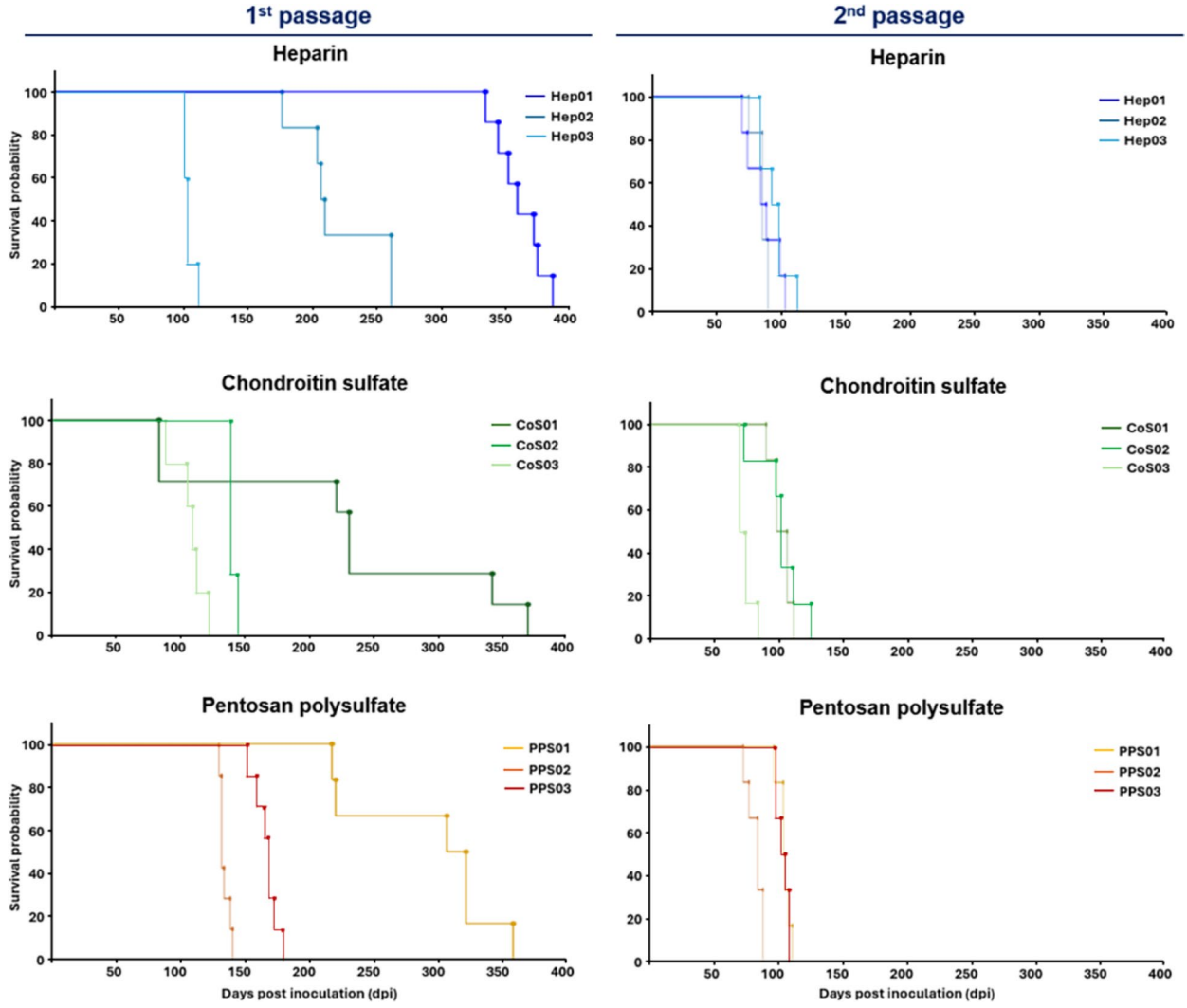

Fig. 4 Kaplan-Meier survival plots of TgVole(I109)1x mice inoculated with spontaneous rec-PrP^{Sc} conformers generated with different polyanionic cofactors. First passage. Groups of 5–8 TgVole(I109)1x mice were inoculated intracerebrally with each of the nine spontaneous rec-PrP^{Sc} conformers. All conformers were infectious with 100% attack rates, except for CoS01 that showed 60% attack rate at first passage but showed markedly different incubation times ranging from 105 ± 2 days (Hep03) to 363 ± 7 days (Hep01). No clear correlation was observed between cofactor type and incubation time, as conformers generated with the same cofactor displayed substantial variability in survival times. Second passage. Mice were inoculated with 1% brain homogenates from terminally ill first-passage animals. Incubation times shortened considerably for all strains, ranging from 74 ± 2 days (CoS03) to 106 ± 2 days (PPS01). The reduction in incubation times varied substantially between conformers, with some showing dramatic decreases (e.g., Hep01: 363→86 days, 76% reduction) while others showed more modest changes (e.g., Hep03: 105→95 days, 10% reduction). The ranking of incubation times changed between passages, indicating adaptation to the host during serial transmission

with a distinct pattern from any of the first passage. Similarly, proportion of non- and monoglycosylated PrP^{res} increases in the preparations in chondroitin sulfate, Cos01 and Cos02 sharing the same proportion, while CoS03 is clearly distinct. In contrast, PPS01, like Ust02 and Ust09 appear to remain mostly unaltered between first and second passage. In agreement with the previous, digestion of all samples with PNGase F, revealed subtle differences in the molecular weight of the unglycosylated PrP^{res} (Supplementary Fig. 8D), PPS02 and Ust02 being clearly distinguishable from the rest in the first passage, and a higher overall variability in the second passage, indicating that most if not all the recombinant prions have adapted through selection or structural evolution during their in vivo propagation.

To confirm the distinct strain properties observed among the nine conformers, we performed comprehensive statistical analysis of the second passage incubation periods. Statistical analysis using Games-Howell's multiple comparisons test revealed significant differences between several conformers in second passage incubation periods (Supplementary Table 1). CoS03 showed significantly shorter incubation periods compared to multiple conformers: Hep02 ($p = 0.0258$), CoS01 ($p = 0.0008$),

PPS01 ($p < 0.0001$), and PPS03 ($p < 0.0001$). Additionally, Hep03 exhibited significantly shorter incubation periods than CoS03 ($p = 0.0383$), while PPS02 showed significantly shorter periods than CoS01 ($p = 0.0037$), PPS01 ($p < 0.0001$), and PPS03 ($p = 0.0002$).

Within conformers derived from the same cofactor, notable significant differences were observed: in the chondroitin sulfate group, CoS03 differed significantly from both CoS01 ($p = 0.0008$) and CoS02 ($p < 0.0001$), while in the pentosan polysulfate group, PPS02 showed significantly shorter incubation periods than both PPS01 ($p < 0.0001$) and PPS03 ($p = 0.0002$). These statistically significant differences confirm that different sulfated cofactors can generate prion strains with distinctive biological properties, even when originating from the same sulfated polysaccharide.

Histopathological analysis confirms generation of distinct prion strains with unique neurotropism patterns

We next performed histopathological characterization of brains from second passage mice to assess lesion profiles and PrP^{Sc} deposition patterns, which are key criteria for strain identification.

Heparin-derived strains: Brains of mice inoculated with conformers generated with heparin showed clear spongiform changes and PrP^{Sc} deposits (Fig. 5). The lesion profile indicated common involvement of the striatum in all three conformers, with incipient spongiosis in the thalamus. Additionally, Hep03 also presented mild vacuolation in the hippocampus and brain stem, with the exception of the hypothalamus. Regarding PrP^{Sc} immunolabeling, these conformers displayed predominantly faint punctate deposition and occasional granular deposits surrounding confluent vacuoles in the striatum. Furthermore, PrP^{Sc} was detected in the thalamus, mesencephalon, and medulla oblongata in mice inoculated with Hep01 and Hep02, although the thalamus was spared in Hep03. Importantly, since Hep01 and Hep02 shared similar incubation periods (86 and 84 dpi, respectively) and displayed a virtually indistinguishable electrophoretic pattern (Fig. 1 and Supplementary Fig. 4) as well as comparable brain tropism, both could be considered the same strain after second passage. In contrast, Hep03 appeared distinct given that this conformer presented a slightly longer incubation period (95 dpi), its electrophoretic pattern showed greater intensity of the diglycosylated band (Supplementary Fig. 8), and it displayed additional affinity for the hippocampus and brain stem. Collectively, these results suggest that Hep03 represents a different strain from Hep01 and Hep02, although additional studies would be needed to confirm this hypothesis.

Chondroitin sulfate-derived strains: CoS01 and CoS02 both had similar incubation periods and comparable lesion profiles, characterized by intense striatal vacuolation and slight involvement of the neocortex and cerebellar cortex with some variability among individuals. Although the spongiform changes appeared similar, the two conformers showed different PrP^{Sc} accumulation patterns. CoS01 presented small florid plaque-like deposits in the striatum and hippocampus and punctate intraneuronal and neuropile staining in the mesencephalon, whereas animals inoculated with CoS02 displayed a more discreet punctate deposition in the striatum and occasional punctate intraneuronal pattern in the thalamus. Most notably, CoS03 showed distinct and unique properties. Hardly any vacuoles were observed, to the point that these animals were considered to have negative histopathology. Nevertheless, these mice still presented punctate intraneuronal and neuropile PrP^{Sc} deposits in their brains in the mesencephalon and medulla oblongata. CoS03 also differed significantly in incubation period, being the fastest conformer in the second passage (74 dpi), and presented different electrophoretic mobility characteristics as well, with reduced accumulation of PrP^{Sc}, which was mainly diglycosylated (Supplementary Fig. 8). These data support the conclusion that three different strains were generated with chondroitin sulfate.

Pentosan polysulfate-derived strains: Regarding the conformers generated with pentosan polysulfate, the three gave rise to clearly distinguishable anatomopathological patterns (Fig. 5). PPS01 was the conformer that caused the most intense spongiform changes, with vacuolation in all brain areas except for the hypothalamus. The spongiosis was accompanied by PrP^{Sc} deposits in the striatum, thalamus, and mesencephalon, including intraneuronal punctate deposits and in the neuropil and perivacuolar granular deposits. PPS02 exhibited neuropathological changes that resembled those caused by Hep01 and Hep02, with moderate vacuolation in the striatum, mild involvement of the brain stem, and mild punctate PrP^{Sc} depositions in the striatum, mesencephalon, and medulla oblongata. In contrast, PPS03 presented slight spongiform changes, detectable only in the thalamus, mesencephalon, medulla oblongata, and cerebellar vermis. Unlike the previous conformers, PPS03 did not trigger spongiosis in the striatum or PrP^{Sc} deposits in this region. Instead, such deposits were located in the brain stem, as faint punctate accumulations in the neuropil. Biochemically, mice inoculated with the three conformers generated with pentosan polysulfate also presented distinct electrophoretic patterns: PPS01 displayed a lower molecular weight diglycosylated band than PPS02 and PPS03. Additionally, all three differed in the intensity and molecular weight of the non-glycosylated band, indicating structural differences (Supplementary Fig. 8). These results demonstrate that three distinct strains were generated with pentosan polysulfate.

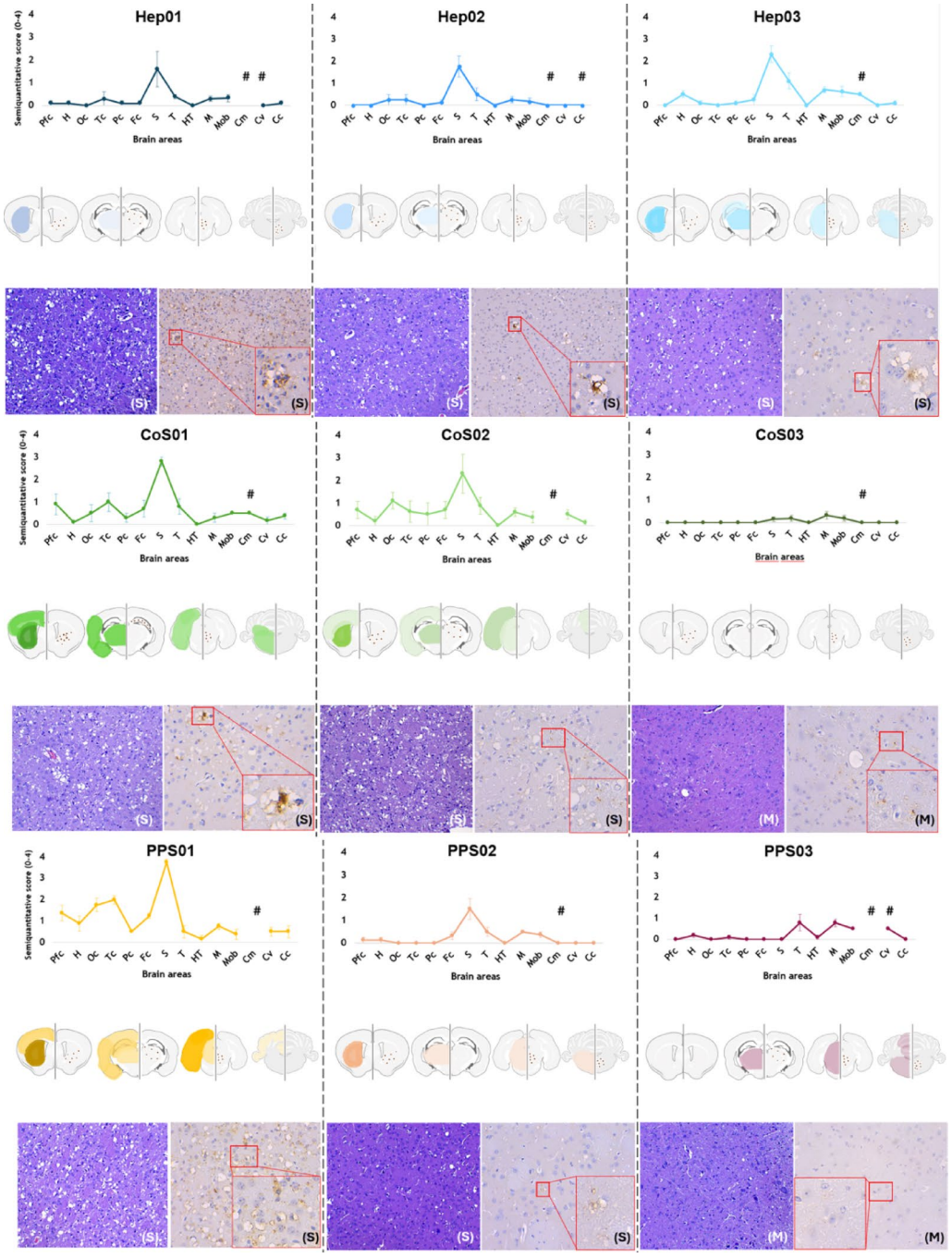

Fig. 5 Histopathological features of TgVole(I109)1x mice inoculated with spontaneous rec-PrP^{Sc} conformers generated with different cofactors. Top panels: Lesion profiles showing mean semiquantitative scores (0–4, vertical axis) of spongiform changes across brain regions for heparin-derived strains (Hep01, Hep02, Hep03), chondroitin sulfate-derived strains (CoS01, CoS02, CoS03), and pentosan polysulfate-derived strains (PPS01, PPS02, PPS03). Brain region abbreviations: Pfc, piriform cortex; H, hippocampus; Oc, occipital cortex; Tc, temporal cortex; Pc, parietal cortex; Fc, frontal cortex; S, striatum; T, thalamus; HT, hypothalamus; M, mesencephalon; Mob, medulla oblongata; Cm, cerebellar nuclei; Cv, cerebellar vermis; Cc, cerebellar cortex. The hash symbol (#) indicates brain areas that could not be examined in all samples. Middle panels: Schematic representation of anatomical distribution of pathological changes based on unilateral brain hemisection analysis. Left diagrams show semiquantitative scores of spongiform lesions, with color intensity indicating severity of vacuolation. Right diagrams show distribution of PrP^{Sc} deposits detected by immunohistochemistry, with colored areas indicating regions of immunoreactivity. Bilateral representation is shown for visualization purposes, though analysis was performed unilaterally. Bottom panels: Representative microscopic images showing hematoxylin-eosin staining (left, spongiform vacuolation) and PrP immunolabeling (right, PrP^{Sc} deposits using 6C2 antibody, epitope at residues 111–118). Letters indicate brain regions: (S) striatum, (M) mesencephalon. Red squares highlight characteristic immunolabeling patterns

Cross-cofactor comparison suggests potential strain convergence despite distinct origins

Comparison of the lesion profiles and incubation periods after second passage among strains generated with different cofactors suggests that some may represent closely related entities despite their distinct origins and electrophoretic mobility patterns observed in the PMSA products. This convergence could be explained by differential protective effects exerted by each cofactor, which might alter PK cleavage sites during in vitro propagation. Alternatively, this phenomenon might reflect the inherent constraints of the bank vole PrP(I109) sequence, which may only be capable of adopting a limited repertoire of stable misfolded conformations, regardless of the initiating cofactor. Most notably, the striking similarity of lesion profiles between Hep01, Hep02, and PPS02, together with their incubation periods of approximately 80 dpi, suggest shared structural characteristics, at least after adaptation to propagation in vivo. Similarly, despite showing different PrP^{Sc} aggregate morphologies, CoS01 and CoS02 displayed almost identical spongiform lesions, which, albeit with greater intensity, were also shared by PPS01. Combined with incubation periods of approximately 100 dpi, these similarities could indicate the formation of highly related strains. These findings suggest that while different cofactors can initiate prion misfolding, the ultimate structural and biological properties may be constrained by the intrinsic folding landscape of the specific PrP sequence employed, as illustrated in Fig. 5.

Discussion

Cryo-EM-based elucidation of several PrP^{Sc} strains [6–10] has shown that it is a PIRIBS amyloid akin to other PrP amyloids purported to be non-infectious [20, 21]. The only difference, although not a trivial one, between these two broad categories of PrP amyloid conformers is that *bona fide* PrP^{Sc}, at least for all the handful of prion strains with atomic level structures available, features a large ~ 90–230 PIRIBS core composed of two lobes, roughly coincident with the two subdomains of the PrP^{C} folded domain (β1-α1-β2 and α2-α3). The N-terminal lobe of PrP^{Sc} also incorporates the ~ 90–120 portion of the highly flexible N-terminal PrP^{C} tail. In turn, amyloids with reduced infectivity feature only one C-terminal lobe [20, 21]. While these single-lobe PrP amyloids propagate easily in vitro like all amyloids, growing evidence shows they can also propagate in the brain, if inoculated intracerebrally, and cause prion disease [19, 43]. However, their capacity to provoke clinical disease is substantially reduced compared to *bona fide* PrP^{Sc}, often requiring two or even three clinically silent passages in suitable animal models [44–46]. This explains why the first spontaneous recombinant prion to be generated had an unusually long incubation time and required a 16x level of PrP overexpression attained in a transgenic model [19]. Therefore, paradoxically, while this prion definitively proved the prion paradigm, it was most likely not a *bona fide* PrP^{Sc} conformer. Thus, its mode of generation (facile incubation of recombinant PrP under denaturing conditions with no cofactors, with simple agitation), has no relevance to the mechanism of genesis of the *bona fide* prions that appear spontaneously in the brain of mammals, including humans. Such spontaneous prions are central to the vast majority of human prion diseases: they directly cause idiopathic cases, likely underlie the transmissible ones such as those seen in kuru and iatrogenic CJD, and may contribute to genetic cases where mutations facilitate spontaneous misfolding, most —if not all— of which can be traced back to an ancestral spontaneous PrP^{Sc} conformer.

After the groundbreaking experiment of Legname et al.., many groups pursued, with little success, methods to generate spontaneous PrP conformers with closer resemblance to brain PrP^{Sc} in terms of infectivity and structure. Given that at the time the structure of PrP^{Sc} had not yet been elucidated, biochemical properties such as a large ~ 90–230 PK-resistant core were used as a structural surrogate. Wang et al. were the first to succeed in generating a spontaneous PrP conformer with the biological and biochemical characteristics of brain PrP^{Sc}. Adapting PMCA, they generated an infectious recombinant PrP product that exhibited an incubation time similar to that of a brain-derived, *bona fide* PrP^{Sc} in wild-type mice and yielded a ~ 90–230 PK-resistant fragment upon treatment with protease. Of note, Wang´s successful reaction mixture contained two anionic cofactors: POPG and RNA [23]. Unfortunately, this and other subsequent PMCA-based methods, all utilizing these and other negatively charged or zwitterionic cofactors such as phosphatidylethanolamine [24, 47–49] exhibited substantial variability, often producing PrP conformers with low or no infectivity and variable biochemical characteristics.

In contrast, our PMSA-based method robustly and reproducibly generates large amounts PK-resistant PrP conformers that demonstrate infectivity in transgenic mice [29, 30]. However, establishing the specific infectivity of these conformers is challenging due to potential conformer mixtures, where highly infectious minor components might coexist with less infectious major populations. This limitation also applies to PrP^{Sc} isolated from infected brain tissue. While we cannot definitively determine specific infectivity values, the abundant production of infectious material and consistent attack rates (100%) suggest that our PMSA-generated conformers possess substantial biological activity.

In its original formulation, the key elements of our PMSA method to generate spontaneous rec-PrP^{Sc} were shaking, glass beads, the detergent Triton X-100, and

dextran sulfate as a cofactor [29, 30]. Here we show that three additional sulfated glycans are equally adept at facilitating robust spontaneous generation of rec-PrP^{Sc}. Therefore, the original cofactor that we used when developing our method, dextran sulfate, is not a *sine qua non* element for success. Neither is the specific original bank vole 109I PrP sequence, which can be replaced by many other PrP sequences [30]. This suggests that, by exclusion, glass beads are the key element in our method. In fact, we already noted during the development of the method that substitution of glass beads with zirconia beads, which are effective at facilitating propagation of pre-formed PrP^{Sc} [27], or beads of other materials such as steel, has a profound impact on the performance of the method [29].

Furthermore, studies carried out by us in parallel to these, and published very recently, showed that complete elimination of any cofactor, as long as glass beads are maintained, allows spontaneous generation of infectious PrP^{Sc}. However, substantially lower efficiency was obtained. Unlike in the dextran-complemented reactions, generation of rec-PrP^{res} was inconsistent across different experiments and replicates. In many cases, after the initial 24 h of PMSA, the protease-resistant products detected featured only low molecular weight fragments (~ 10 kDa and < 5 kDa), which evolved in subsequent rounds into the electrophoretic pattern associated with recombinant *bona fide* PrP^{Sc} prions, characterized by a 16 kDa fragment [32]. This means that while the glass beads are the only component that cannot be eliminated, robust and consistent spontaneous conversion of PrP^{C} to PrP^{Sc} requires combining them with a sulfated glycan, which needs not be dextran sulfate.

Our data show that heparin, chondroitin sulfate, and pentosan polysulfate also share with dextran sulfate the capacity to facilitate spontaneous generation of a diversity of PrP^{Sc} strains. This is an important feature of our method, not shared by earlier methods which generate only one PrP^{Sc} strain [25]. It is known that brains affected by spontaneous prion disease may harbor more than one prion strain, which must necessarily have emerged together [50, 51]. In fact, a notion widely held in the prion field is that pure prion strains rarely exist; rather, populations of slightly different PrP^{Sc} conformers termed "quasi-species" predominate, often with a main component and many minor ones [42]. Our method thus offers a unique tool to study the emergence of such quasi-species.

Our results do not provide any evidence of correlations between a given cofactor and the biochemical (and therefore structural) and biological properties of the spontaneous PrP^{Sc} conformers whose emergence it facilitates. As shown in Fig. 1 and Supplementary Fig. 4, PK-resistant patterns seem randomly distributed across the PrP^{Sc} conformers obtained with the three cofactors (four, if we include the two strains previously obtained with dextran sulfate and used for comparative purposes). The pattern of a PrP^{Sc} strain obtained with one given cofactor is often more similar to the pattern of a strain obtained with a different cofactor than to the patterns of strains obtained with the same cofactor. The same is true for incubation times. Mean incubation times in the first passage did not vary significantly across cofactors, and within each cofactor group, very large differences were seen. Furthermore, strains showing relatively similar PK-resistant patterns, such as Hep01 and Hep03 or PPS02 and Hep02, exhibited very discordant incubation times among themselves at first passage, although this could be attributed to differences in the titer of each PMSA product inoculated. We could not derive any correlation between the presence or absence of a given PK-resistant fragment, or the relative intensity of the corresponding electrophoretic bands, and incubation times. With respect to the second passage, there were reductions in incubation time for every strain, as expected. Again, however, no pattern could be established. Strain Hep01 changed from 363 ± 7 to 86 ± 5 days, whereas Hep03 changed from 105 ± 2 to 95 ± 4 days, suggesting that the transmission barrier was easily surmounted in the second passage regardless of its original magnitude. All of this suggests that the biological properties of a given spontaneous rec-PrP^{Sc} conformer must be subtly encoded in its structure in such a way that the biochemical methods used in this study to assess and compare differences and similarities between the different conformers do not have sufficient resolution to allow for definitive conclusions. The high variability in PK-resistant fragment patterns and their lack of correlation with biological features may involve cofactor-PrP^{Sc} interactions. Recent cryo-EM structures of hamster and murine prions reveal poorly resolved densities near polybasic stretches (such as the K_{101}-K_{110} cluster) [6, 8] that are replaced by phosphotungstic acid (PTA) in purified strains [9], suggesting these densities represent endogenous polyanionic cofactors—likely GAGs, nucleic acids, or lipids. Previous studies demonstrate that distinct polyanionic molecules exhibit varying PrP^{C}-binding affinities and effects on prion misfolding in vitro [52, 53]. Since these cofactors are PK-resistant, they can sterically protect nearby cleavage sites from protease digestion, as demonstrated experimentally for dextran sulfate-associated recombinant prions [32]. Therefore, the observed electrophoretic differences might reflect varying cofactor binding patterns and protective effects rather than intrinsic structural variations among PMSA products. This mechanism could explain why biochemically distinct preparations converge upon in vivo transmission, highlighting the need for complementary characterization methods beyond electrophoretic analysis.

The quantitative morphological analysis of fibers visualized by TEM and negative staining presented here provides objective validation for the morphological diversity observed qualitatively through biochemical and biological characterization. The identification of five distinct morphotypes demonstrates that sulfated glycan cofactors can generate not only biochemically distinct conformers but also morphologically distinguishable fibril populations. The fact that different cofactors can produce similar morphotypes (e.g., Morphotype 1 across multiple conformers) while the same cofactor can generate distinct patterns (e.g., Hep01 vs. Hep02) further suggests that the relationship between cofactor chemistry and final fibril morphology is complex and likely influenced by stochastic nucleation events during PMSA. This morphological diversity may reflect subtle differences in PIRIBS core organization that are not readily apparent in biochemical analyses but could contribute to the distinct biological properties observed in vivo. Without doubt, resolution of the structures at an atomistic level by means of cryo-EM (ongoing studies) will provide answers. Previous studies using shaking or sonication-based methods with single cofactors have generated apparently stable conformations that eventually converged into a single strain [24, 54], contrasting with our PMSA results using dextran sulfate [29] or the three polyanionic cofactors described herein. Among the main differences with respect to the previous methods is the inclusion of glass beads that is critical to achieve spontaneous rec-PrP misfolding in our system together with the cofactor, which could raise doubts on their role in generating and keeping stable the distinct conformers characterized here. Glass beads could somehow overcome the effect of specific cofactors on defining and maintaining their biological properties, which in other cases have been demonstrated to converge to a predominant conformation. Nonetheless, the fact that the electrophoretic mobility pattern and PK-resistant fragments of our recombinant prions remain stable throughout their propagation in PMSA using zirconia silica beads (also observed in Eraña et al., 2023 [29]), suggests that the main drivers of the conformational differences in this system are the distinct cofactors, rather than the use of a specific type of beads.

GAGs, and more specifically heparin, have long been known to facilitate spontaneous generation of neurodegenerative disease-relevant amyloids in vivo, particularly α-synuclein (α-syn) [55, 56] and tau [57, 58]. Besides acting as a scaffold for the assembly of the amyloid, negatively charged GAGs counter the stacked, electrostatically repulsive positive charges of similar basic residues in the PIRIBS. A recent cryo-EM-based study of α-syn fibrils in complex with heparin showed that heparin chains extend along the α-synuclein protofilament axis, with sulfonic acid groups forming salt bridges with two positively charged grooves formed by Lys43 and Lys45, and Lys58, Lys60, and Lys97, respectively (termed conformer P1 by the authors). However, heparin can also interact with Lys80, in which case the fold of the α-synuclein monomer changes and a different polymeric conformer, termed P4, is generated, with a surface-exposed stack of lys80 residues whose repelling positive charges are neutralized by heparin (termed P4). Two additional conformers, P2 and P3, can also emerge. P2 is characterized by lateral association of two P1-like protofilaments [56]. The study did not reveal what causes emergence of one or other amyloid strain. Another contemporary study solved the atomistic structures of α-synuclein fibers extracted from the brains of patients that had suffered from Parkinson´s disease and multiple system atrophy (MSA). It showed that filaments with a "Lewy fold" feature a non-peptidic density embedded in the characteristic Lys32, Lys34, Tyr39, Lys43, and Lys45 groove of the filament, whereas two strains with "MSA fold" also contained non-peptidic densities at the interface of two protofilaments, surrounded by Lys43 and Lys45 of each of the two α-synuclein units [59].

Both studies highlight the scaffolding capacity of heparin, likely sustaining polymerization of α-synuclein to generate more than one conformer. Taking all this into consideration, it is tempting to speculate that perhaps heparin (and the other two GAGs used in our experiments) might bind to the Lys-rich patch K_{101}PSKPKTNIK_{110} within the unfolded N-terminal domain of PrP^{C}, providing a scaffold for several such patches and their immediate unfolded N- and C-terminal residues to nucleate into a short PIRIBS (Fig. 6). Eventually, the entire ~ 90–121 tail stretch would be converted to the PIRIBS conformation. It has been previously shown that heparin binds the flexible N-terminal tail of recombinant PrP^{C} through a pH-dependent interaction that is strongest at acidic pH values and sharply decreases at pH values above 7.5. At pH 6.5, the interaction was followed by the formation of PrP oligomeric complexes [60]. It is known that the central portion of PrP^{C}, rich in amyloidogenic residues, has a high tendency to fibrillize into an amyloid conformation. In fact, a PrP106-126 peptide and its amyloid fibrils were used for a long time as a surrogate for PrP^{Sc} in dozens of studies in the 1990´s and 2000´s [61]. Paradoxically, when the whole PrP sequence, 23–230, is unfolded under denaturing conditions, fibrillization proceeds through the C-terminus and amyloids with a ~ 170–230 PIRIBS core are formed [20, 21, 62, 63]. This is likely a consequence of the effect of the Cys176-Cys214 disulfide bond as a staple that fixes the 176–214 loop, restricting its motion and positioning it as a nucleation core that outcompetes the N-terminal ~ 90–120 region. However, in the presence of a fully folded globular

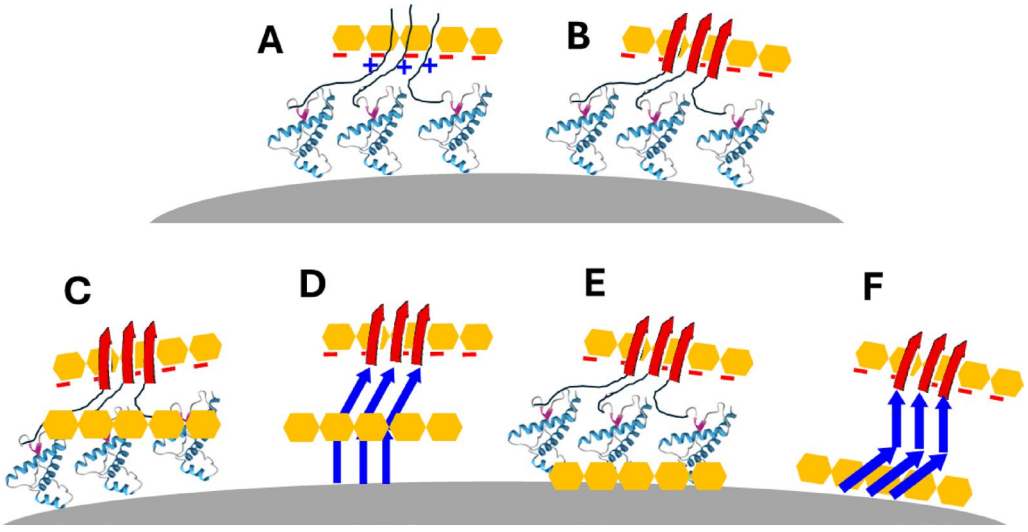

Fig. 6 Hypothetical modulation by GAGs of spontaneous emergence of distinct strains of rec-PrP^{Sc}through PMSA. **A**: PrP^{C} molecules adsorb to glass beads [29] generating a high local concentration (the ~ 23–90 segments that are disordered and PK-sensitive in both PrP^{C} and PrP^{Sc} are omitted for simplicity). Negatively charged GAGs interact with the positively charged $\mathbf{K}_{101}$PSKPKTNIK$_{110}$ patch within their unfolded 90–120 N-terminal tails, affording a nucleation scaffold. **B**: An N-terminal PIRIBS block is formed. **C**: Additional GAG chains adsorbed to the folded ~ 121–231 domains of PrP^{C} molecules help align them and contribute to their unfolding, facilitating their refolding into a C-terminal PIRIBS domain **D**. An alternative binding pose of the GAG **E**, either because of an alternative binding interaction or because it is a different GAG with a different structure, nucleates and scaffolds a distinctly different conformation of the C-terminal PIRIBS domain **F**

~ 121–231 domain as in our experiments, such competition is not possible. Furthermore, the high local concentration of PrP^{C} molecules adsorbed to the surface of glass beads [29] would favor nucleation around the GAG linear polymer (Fig. 6).

Continuing with the speculation, once the N-terminal PIRIBS has been formed, the attached globular domains will need to unfold and refold into a C-terminal PIRIBS lobe. Using solution NMR, Vieira et al.. have shown that heparin binds to both the unfolded N-terminus at pH 7 and also to a specific site of the globular domain of mouse PrP at pH 5 [64]. While PMSA is carried out at pH = 7.4 in phosphate buffer, the glass beads used have been acid-washed by the manufacturer, and their surface might provide acidic microenvironments. Of note, when acid-washed beads were replaced by regular glass beads not subjected to acid washing, yields of spontaneous PrP^{Sc} generation decreased [29]. Binding of heparin (and other sulfated glycans) to the folded domain of PrP^{C} might facilitate its unfolding or perhaps chaperone the process so as to prevent futile interactions of partially unfolding intermediates competing with ordered stacking, leading to completion of a full ~90–231 PIRIBS core (Fig. 6).

Our results demonstrate that sulfated glycans not only facilitate spontaneous conversion of PrP^{C} into PrP^{Sc} but also enable the emergence of different, possibly closely related, but distinct PrP^{Sc} strains (see a summary of the differential properties of each preparation evaluated throughout this work in Supplementary Fig. 9). This is of clear relevance to spontaneous emergence of PrP^{Sc} in vivo: sulfated glycans (GAGs) such as heparan sulfate (of which heparin is a mimic), and others, are present in cell membranes and are very likely to interact with PrP^{C} and with nascent spontaneous PrP^{Sc}. Besides their putative role in facilitating spontaneous emergence of PrP^{Sc}, already discussed, GAGs have been shown to play a relevant role in the process of interaction of PrP^{Sc} with cells, which is key to their toxicity. Experiments *in cellula* have shown that heparan sulfate is necessary for PrP^{Sc} formation in ScN2a cells and acts as a cellular receptor for purified infectious prions [65–67]. Furthermore, heparan sulfate is found in prion plaques in brain sections from patients affected by prion disease and prion-infected mice [68, 69]. It is therefore not surprising that shortening heparan sulfate chains through transgenic exostosin-1 haploinsufficiency prolongs survival and reduces parenchymal plaques in a model of prion disease [34]. On the other hand, paradoxically, some GAG mimetics have been proposed as anti-prion therapy [70–73]. This apparent contradiction is likely explained by the aforementioned dual action of GAGs and their mimetics: once PrP^{Sc} exists in the body, externally administered GAGs might compete with cellular GAGs for binding sites, preventing their interaction with cells and reducing their pathogenicity. Additionally, previous cell culture studies have shown that sulfated glycans can inhibit PrP^{Sc} accumulation by altering PrP^{C} subcellular localization through clumping and internalization mechanisms, highlighting the complex and context-dependent nature of GAG-prion interactions [67, 70].

In summary, this study demonstrates that sulfated glycans such as heparin, chondroitin sulfate, and pentosan polysulfate are potent cofactors capable of driving the spontaneous generation of multiple, structurally and biologically distinct recombinant prion strains. Using PMSA, we reproducibly obtained nine infectious rec-PrP^{Sc} conformers with distinct protease resistance profiles, fibril morphologies, incubation times, and neuroanatomical tropisms, confirming their classification as bona fide prion strains. Notably, some strains with similar properties arose from different cofactors, while multiple strains could also emerge from a single cofactor, highlighting both the permissiveness and selectivity of glycan-driven prion strain diversification. These findings offer significant insights into the molecular determinants of prion strain diversity and support the hypothesis that spontaneous emergence of distinct prion strains in vivo may be influenced by the presence and nature of endogenous polyanionic cofactors.

Supplementary Information

The online version contains supplementary material available at https://doi.org/10.1186/s40478-025-02175-w.

Supplementary Material 1.

Supplementary Material 2.

Acknowledgements

The authors would like to thank the following for their assistance and support: the IKERBasque Foundation; the vivarium, IT service and maintenance departments of CIC bioGUNE for their outstanding assistance; the Electron Microscopy Platform from CIC bioGUNE for excellent service and assistance; María de la Sierra Espinar and the rest of the IRTA-CReSA BSL3 facility personnel for their excellent technical support; and the staff of the biocontainment units at Neiker and CEBEGA for their excellent care and maintenance of the animals. The authors would also like to acknowledge the work from past laboratory members of the Prion Research Lab from CIC bioGUNE, that despite not directly involved in the manuscript have contributed along the years to the development of all the methods and techniques currently used in the laboratory.The present address of Nuria L. Lorenzo is: Galician Advanced Therapies Manufacturing Center, Galaria, Santiago de Compostela, Spain. And the present address of Sonia Veiga is: Food and Health Omics Lab, Faculty of Sciences, Ourense campus, University of Vigo, Spain.

Author contributions

Conception and design of the study was done by J.C., J.R.R. and H.E.; N.L.L., H.E., J.M.C., C.M.D-D, L.C. and S.V. performed the biochemical experiments and the analysis of biological samples, all participating in data acquisition, analysis and interpretation; N.L.L., L.P., S.V. and S.B. performed the Mass Spectrometry experiments including material preparation, data acquisition, analysis and interpretation; N.L.L., H.E., E.V., S.G., M.G. performed the in vivo studies and anatomopathological analyses; N.L.L., H.E., J.R.R. and J.C. drafted the initial versions of the manuscript and all authors reviewed and approved the submitted version.

Funding

The present work was partially funded by the following grants awarded by "Agencia Estatal de Investigación, Ministerio de Ciencia e Innovación" (Spanish Government): PID2024-160022OB-I00, PID2021-122201OB-C21 (granted to J.C.), PID2021-122201OB-C22 (granted to E.V.), and PID2020-117465GB-I00 (granted to J.R.R.), funded by MCIN/AEI/10.13039/501100011033 and co-financed by the European Regional Development Fund (ERDF).

Data availability

All data generated or analysed during this study are included in this published article and its supplementary information files.

Declarations

Ethics approval and consent to participate

Mouse experiments were performed at multiple research facilities: CIC bioGUNE, Centro de Biomedicina Experimental (CEBEGA) of the University of Santiago de Compostela, Neiker—Basque Institute for Agricultural Research and Development, and IRTA-CReSA Animal Health Research Center. These procedures were approved by the respective institutional ethics committees with the following project codes: CIC bioGUNE (P-CBG-CBBA-0314 and 15,005/16/006), CEBEGA (15012/2023/002), Neiker (NEIKER-OEBA-2021-003), and IRTA-CReSA (5767, 11926 and 1124M2R). All experimental procedures performed until 2013 in Spain complied with the "Real Decreto 1201/2005 de 10 de Octubre" and "Real Decreto 214/1997 de 30 de Julio" on animal protection for experimental purposes, and those carried out from 2013 onwards complied with "Real Decreto 53/2013 de 1 de febrero" on protection of animals used for experimentation and other scientific purposes, which is based on European Directive 2010/63/EU on Laboratory Animal Protection.

Competing interests

Authors H.E. and J.M.C. are employed by the commercial company ATLAS Molecular Pharma SL. This does not alter our adherence to the Journal's policies on sharing data and materials and did not influence in any way the work reported in this manuscript, given that the company had no role in study design, funding, and data analysis. The rest of the authors declare no competing interests.

Author details

[1]CIMUS Biomedical Research Institute, University of Santiago de Compostela-IDIS, Santiago de Compostela, Spain
[2]Prion Research Lab, CIC BioGUNE, Basque Research and Technology Alliance (BRTA), Derio, Spain
[3]Centro de Investigación Biomédica en Red de Enfermedades Infecciosas (CIBERINFEC), Carlos III National Health Institute, Madrid, Spain
[4]ATLAS Molecular Pharma S. L, Derio, Spain
[5]Unitat mixta d'Investigació IRTA-UAB en Sanitat Animal, Centre de Recerca en Sanitat Animal (CReSA), Campus de la Universitat Autònoma de Barcelona (UAB), Bellaterra, Catalonia, Spain
[6]IRTA. Programa de Sanitat Animal, Centre de Recerca en Sanitat Animal (CReSA), Universitat Autònoma de Barcelona (UAB), Campus, Bellaterra, Catalonia, Spain
[7]Proteomics Unit, Instituto de Investigaciones Sanitarias de Santiago (IDIS), Santiago de Compostela, Spain
[8]Animal Health Department, NEIKER-Basque Institute for Agricultural Research and Development , Basque Research and Technology Alliance (BRTA), Derio, Spain
[9]IKERBASQUE, Basque Foundation for Science, Bilbao, Spain

Received: 12 June 2025 / Accepted: 23 October 2025
Published online: 03 December 2025

References

1. Prusiner SB, Prions (1998) Proc Natl Acad Sci 95:13363–13383
2. Aguzzi A, Calella AM (2009) Prions: protein aggregation and infectious diseases. Physiol Rev 89:1105–1152
3. Prusiner SB (1982) Novel proteinaceous infectious particles cause scrapie. Science 216:136–144
4. Mabbott NA (2017) Chapter ten immunology of prion protein and prions. Prog Mol Biol Transl Sci 150:203–240
5. Prusiner SB, DeArmond SJ (1991) Molecular biology and pathology of scrapie and the prion diseases of humans. Brain Pathol 1:297–310
6. Kraus A, Hoyt F, Schwartz CL, Hansen B, Artikis E, Hughson AG et al (2021) High-resolution structure and strain comparison of infectious mammalian prions. Mol Cell 81:4540–4551e6

7. Hoyt F, Alam P, Artikis E, Schwartz CL, Hughson AG, Race B et al (2022) Cryo-EM of prion strains from the same genotype of host identifies conformational determinants. PLOS Pathog 18:e1010947
8. Hoyt F, Standke HG, Artikis E, Schwartz CL, Hansen B, Li K et al (2022) Cryo-EM structure of anchorless RML prion reveals variations in shared motifs between distinct strains. Nat Commun 13:4005
9. Manka SW, Zhang W, Wenborn A, Betts J, Joiner S, Saibil HR et al (2022) 2.7 Å cryo-EM structure of ex vivo RML prion fibrils. Nat Commun 13:4004
10. Manka SW, Wenborn A, Betts J, Joiner S, Saibil HR, Collinge J et al (2023) A structural basis for prion strain diversity. Nat Chem Biol 19:607–613
11. Prusiner SB, Scott MR, DeArmond SJ, Cohen FE (1998) Prion Protein Biology Cell 93:337–348
12. Donne DG, Viles JH, Groth D, Mehlhorn I, James TL, Cohen FE et al (1997) Structure of the Recombinant full-length hamster prion protein PrP(29–231): the N terminus is highly flexible. Proc Natl Acad Sci 94:13452–13457
13. Hornemann S, Korth C, Oesch B, Riek R, Wider G, Wüthrich K et al (1997) Recombinant full-length murine prion protein, mPrP(23–231): purification and spectroscopic characterization. FEBS Lett 413:277–281
14. Prion (2024) Conference Abstracts. Prion. 2024;18:1–47
15. O'Brien EP, Okamoto Y, Straub JE, Brooks BR, Thirumalai D (2009) Thermodynamic perspective on the Dock – Lock growth mechanism of amyloid fibrils. J Phys Chem B 113:14421–14430
16. Guijarro JI, Sunde M, Jones JA, Campbell ID, Dobson CM (1998) Amyloid fibril formation by an SH3 domain. Proc Natl Acad Sci 95:4224–4228
17. GRIFFITH JS (1967) Nature of the scrapie agent: Self-replication and scrapie. Nature 215:1043–1044
18. Come JH, Fraser PE, Lansbury PT (1993) A kinetic model for amyloid formation in the prion diseases: importance of seeding. Proc Natl Acad Sci 90:5959–5963
19. Legname G, Baskakov IV, Nguyen H-OB, Riesner D, Cohen FE, DeArmond SJ et al (2004) Synth Mammalian Prions Sci 305:673–676
20. Wang L-Q, Zhao K, Yuan H-Y, Wang Q, Guan Z, Tao J et al (2020) Cryo-EM structure of an amyloid fibril formed by full-length human prion protein. Nat Struct Mol Biol 27:598–602
21. Wang L-Q, Zhao K, Yuan H-Y, Li X-N, Dang H-B, Ma Y et al (2021) Genetic prion disease–related mutation E196K displays a novel amyloid fibril structure revealed by cryo-EM. Sci Adv 7:eabg9676
22. Deleault NR, Harris BT, Rees JR, Supattapone S (2007) Formation of native prions from minimal components in vitro. Proc Natl Acad Sci 104:9741–9746
23. Wang F, Wang X, Yuan C-G, Ma J (2010) Generating a prion with bacterially expressed Recombinant prion protein. Science 327:1132–1135
24. Deleault NR, Walsh DJ, Piro JR, Wang F, Wang X, Ma J et al (2012) Cofactor molecules maintain infectious conformation and restrict strain properties in purified prions. Proc Natl Acad Sci [Internet]. ;109:E1938–46. Available from: http://www.pnas.org/cgi/doi/https://doi.org/10.1073/pnas.1206999109
25. Supattapone S (2014) Synthesis of High Titer Infectious Prions with Cofactor Molecules*. J Biol Chem [Internet]. ;289:19850–4. Available from: http://pubmed.gov/24860097
26. Miller MB, Wang DW, Wang F, Noble GP, Ma J, Woods VL et al (2013) Cofactor Molecules Induce Structural Transformation during Infectious Prion Formation. Structure [Internet]. ;21:2061–8. Available from: https://doi.org/10.1016/j.str.2013.08.025
27. Eraña H, Charco JM, Bari MAD, Díaz-Domínguez CM, López-Moreno R, Vidal E et al (2019) Development of a new largely scalable in vitro prion propagation method for the production of infectious recombinant prions for high resolution structural studies. PLoS Pathog [Internet]. ;15:e1008117. Available from: https://doi.org/10.1371/journal.ppat.1008117
28. Fernández-Borges N, Bari MAD, Eraña H, Sánchez-Martín M, Pirisinu L, Parra B et al (2017) Cofactors influence the biological properties of infectious recombinant prions. Acta Neuropathol [Internet]. ;135:179–99. Available from: http://link.springer.com/https://doi.org/10.1007/s00401-017-1782-y
29. Eraña H, Díaz-Domínguez CM, Charco JM, Vidal E, González-Miranda E, Pérez-Castro MA et al (2023) Understanding the key features of the spontaneous formation of Bona Fide prions through a novel methodology that enables their swift and consistent generation. Acta Neuropathol Commun 11:145
30. Eraña H, Sampedro-Torres-Quevedo C, Charco JM, Díaz-Domínguez CM, Peccati F, San-Juan-Ansoleaga M et al (2024) A protein misfolding shaking Amplification-based method for the spontaneous generation of hundreds of Bona Fide prions. Nat Commun 15:2112
31. Fernández-Borges N, Eraña H, Elezgarai SR, Harrathi C, Venegas V, Castilla J, Prions (2017) Methods and Protocols. Methods Mol Biol [Internet]. ;1658:205–16. Available from: http://pubmed.gov/28861792
32. Pérez-Castro MÁ, Eraña H, Vidal E, Charco JM, Lorenzo NL, Gonçalves-Anjo N et al (2025) Cofactors facilitate Bona Fide prion misfolding in vitro but are not necessary for the infectivity of Recombinant murine prions. PLOS Pathog 21:e1012890
33. Vidal E, Sánchez-Martín MA, Eraña H, Lázaro SP, Pérez-Castro MA, Otero A et al (2022) Bona Fide atypical scrapie faithfully reproduced for the first time in a rodent model. Acta Neuropathol Commun 10:179
34. Aguilar-Calvo P, Sevillano AM, Bapat J, Soldau K, Sandoval DR, Altmeppen HC et al (2019) Shortening heparan sulfate chains prolongs survival and reduces parenchymal plaques in prion disease caused by mobile, ADAM10-cleaved prions. Acta Neuropathol [Internet]. ;139:527–46. Available from: http://link.springer.com/https://doi.org/10.1007/s00401-019-02085-x
35. Vázquez-Fernández E, Alonso J, Pastrana MA, Ramos A, Stitz L, Vidal E et al (2012) Structural Organization of Mammalian Prions as Probed by Limited Proteolysis. Baskakov IV, editor. PLoS ONE [Internet]. ;7:e50111. Available from: https://doi.org/10.1371/journal.pone.0050111
36. Silva CJ, Vázquez-Fernández E, Onisko B, Requena JR (2015) Proteinase K and the structure of prpsc: the good, the bad and the ugly. Virus Res 207:120–126
37. Sevillano AM, Fernández-Borges N, Younas N, Wang F, Elezgarai SR, Bravo S et al (2018) Recombinant PrPSc shares structural features with brain-derived prpsc: insights from limited proteolysis. PLoS Pathog 14:e1006797
38. Sajnani G, Pastrana MA, Dynin I, Onisko B, Requena JR (2008) Scrapie prion protein structural constraints obtained by limited proteolysis and mass spectrometry. J Mol Biol 382:88–98
39. Zanusso G, Farinazzo A, Prelli F, Fiorini M, Gelati M, Ferrari S et al (2004) Identification of distinct N-terminal truncated forms of prion protein in different Creutzfeldt-Jakob disease Subtypes*. J Biol Chem 279:38936–38942
40. Kocisko DA, Lansbury PT, Caughey B (1996) Partial unfolding and refolding of Scrapie-Associated prion protein: evidence for a critical 16-kDa C-Terminal domain †. Biochemistry 35:13434–13442
41. Zou W-Q, Capellari S, Parchi P, Sy M-S, Gambetti P, Chen SG (2003) Identification of novel proteinase K-resistant C-terminal fragments of PrP in Creutzfeldt-Jakob Disease*. J Biol Chem 278:40429–40436
42. Weissmann C, Li J, Mahal SP, Browning S (2011) Prions on the move. EMBO Rep [Internet]. ;12:1109–17. Available from: https://doi.org/10.1038/embor.2011.192
43. Rezaei H, Martin D, Herzog L, Reine F, Moreno AM, Moudjou M et al (2024) Species barrier as molecular basis for adaptation of synthetic prions with N-terminally truncated PrP. FEBS J 291:5051–5076
44. Klimova N, Makarava N, Baskakov IV (2015) The diversity and relationship of prion protein self-replicating states. Virus Res [Internet]. ;207:113–9. Available from: http://linkinghub.elsevier.com/retrieve/pii/S0168170214004067
45. Makarava N, Kovacs GG, Bocharova O, Savtchenko R, Alexeeva I, Budka H et al (2010) Recombinant prion protein induces a new transmissible prion disease in wild-type animals. Acta Neuropathol 119:177–187
46. Makarava N, Kovacs GG, Savtchenko R, Alexeeva I, Budka H, Rohwer RG et al (2011) Genesis of Mammalian Prions: From Non-infectious Amyloid Fibrils to a Transmissible Prion Disease. Supattapone S, editor. PLoS Pathog [Internet]. 7:e1002419. Available from: https://doi.org/10.1371/journal.ppat.1002419
47. Deleault NR, Piro JR, Walsh DJ, Wang F, Ma J, Geoghegan JC et al (2012) Isolation of phosphatidylethanolamine as a solitary cofactor for prion formation in the absence of nucleic acids. Proc Natl Acad Sci. 109:8546–51. Available from: https://doi.org/10.1073/pnas.1204498109
48. Timmes AG, Moore RA, Fischer ER, Priola SA (2013) Recombinant Prion Protein Refolded with Lipid and RNA Has the Biochemical Hallmarks of a Prion but Lacks In Vivo Infectivity. Chiesa R, editor. PLoS ONE [Internet]. ;8:e71081. Available from: https://doi.org/10.1371/journal.pone.0071081
49. Wang F, Wang X, Orrú CD, Groveman BR, Surewicz K, Abskharon R et al (2017) Self-propagating, protease-resistant, Recombinant prion protein conformers with or without in vivo pathogenicity. PLoS Pathog 13:e1006491
50. Notari S, Capellari S, Langeveld J, Giese A, Strammiello R, Gambetti P et al (2007) A refined method for molecular typing reveals that co-occurrence of PrPSc types in Creutzfeldt–Jakob disease is not the rule. Lab Investig 87:1103–1112
51. Polymenidou M, Stoeck K, Glatzel M, Vey M, Bellon A, Aguzzi A (2005) Coexistence of multiple PrPSc types in individuals with Creutzfeldt-Jakob disease. Lancet Neurol 4:805–814
52. Wong C, Xiong L, Horiuchi M, Raymond L, Wehrly K, Chesebro B et al (2001) Sulfated glycans and elevated temperature stimulate PrPSc-dependent cell-free formation of protease-resistant prion protein. EMBO J [Internet]. ;20:377–86. Available from: http://emboj.embopress.org/cgi/doi/https://doi.org/10.1093/emboj/20.3.377

53. Caughey B, Brown K, Raymond GJ, Katzenstein GE, Thresher W (1994) Binding of the protease-sensitive form of PrP (prion protein) to sulfated glycosaminoglycan and congo red [corrected]. J Virol 68:2135–2141
54. Walsh DJ, Schwind AM, Noble GP, Supattapone S (2023) Conformational diversity in purified prions produced in vitro. PLOS Pathog 19:e1011083
55. Cohlberg JA, Li J, Uversky VN, Fink AL (2002) Heparin and other glycosaminoglycans stimulate the formation of amyloid fibrils from α-Synuclein in vitro †. Biochemistry 41:1502–1511
56. Tao Y, Sun Y, Lv S, Xia W, Zhao K, Xu Q et al (2022) Heparin induces α-synuclein to form new fibril polymorphs with attenuated neuropathology. Nat Commun 13:4226
57. Townsend D, Fullwood NJ, Yates EA, Middleton DA (2020) Aggregation kinetics and filament structure of a Tau fragment are influenced by the sulfation pattern of the cofactor heparin. Biochemistry 59:4003–4014
58. Scheres SH, Zhang W, Falcon B, Goedert M (2020) Cryo-EM structures of Tau filaments. Curr Opin Struct Biol 64:17–25
59. Yang Y, Shi Y, Schweighauser M, Zhang X, Kotecha A, Murzin AG et al (2022) Structures of α-synuclein filaments from human brains with lewy pathology. Nature 610:791–795
60. González-Iglesias R, Pajares MA, Ocal C, Espinosa JC, Oesch B, Gasset M (2002) Prion protein interaction with glycosaminoglycan occurs with the formation of oligomeric complexes stabilized by Cu(II) bridges. J Mol Biol 319:527–540
61. Forloni G, Chiesa R, Bugiani O, Salmona M, Tagliavini F (2019) Review: PrP 106-126-25 years after. Neuropathol Appl Neurobiol 45:430–440
62. Tycko R, Savtchenko R, Ostapchenko VG, Makarava N, Baskakov IV (2010) The α-Helical C-Terminal domain of Full-Length Recombinant PrP converts to an In-Register parallel β-Sheet structure in PrP fibrils: evidence from solid state nuclear magnetic resonance. Biochemistry 49:9488–9497
63. Müller H, Brener O, Andreoletti O, Piechatzek T, Willbold D, Legname G et al (2014) Progress towards structural understanding of infectious sheep PrP-amyloid. Prion [Internet]. ;8:344–58. Available from: http://pubmed.gov/25482596
64. Vieira TCRG, Reynaldo DP, Gomes MPB, Almeida MS, Cordeiro Y, Silva JL (2011) Heparin binding by murine Recombinant prion protein leads to transient aggregation and formation of RNA-Resistant species. J Am Chem Soc 133:334–344
65. Caughey B, Raymond GJ (1993) Sulfated polyanion inhibition of scrapie-associated PrP accumulation in cultured cells. J Virol [Internet]. ;67:643–50. Available from: http://jvi.asm.org/content/67/2/643.short
66. Horonchik L, Tzaban S, Ben-Zaken O, Yedidia Y, Rouvinski A, Papy-Garcia D et al (2005) Heparan sulfate is a cellular receptor for purified infectious Prions. J Biol Chem 280:17062–17067
67. Ben-Zaken O, Tzaban S, Tal Y, Horonchik L, Esko JD, Vlodavsky I et al (2003) Cellular Heparan sulfate participates in the metabolism of Prions. J Biol Chem 278:40041–40049
68. McBride PA, Wilson MI, Eikelenboom P, Tunstall A, Bruce ME (1998) Heparan sulfate proteoglycan is associated with amyloid plaques and neuroanatomically targeted PrP pathology throughout the incubation period of Scrapie-Infected mice. Exp Neurol 149:447–454
69. Snow AD, Wight TN, Nochlin D, Koike Y, Kimata K, DeArmond SJ et al (1990) Immunolocalization of Heparan sulfate proteoglycans to the prion protein amyloid plaques of Gerstmann-Straussler syndrome, Creutzfeldt-Jakob disease and scrapie. Lab Investig J Tech Methods Pathol 63:601–611
70. Adjou KT, Simoneau S, Salès N, Lamoury F, Dormont D, Papy-Garcia D et al (2003) A novel generation of heparan sulfate mimetics for the treatment of prion diseases. J Gen Virol [Internet]. ;84:2595–603. Available from: http://vir.sgmjournals.org/cgi/doi/https://doi.org/10.1099/vir.0.19073-0
71. Doh-ura K, Ishikawa K, Murakami-Kubo I, Sasaki K, Mohri S, Race R et al (2004) Treatment of Transmissible Spongiform Encephalopathy by Intraventricular Drug Infusion in Animal Models. J Virol [Internet]. ;78:4999–5006. Available from: http://jvi.asm.org/cgi/doi/https://doi.org/10.1128/JVI.78.10.4999-5006.2004
72. Farquhar CF, Dickinson AG (1986) Prolongation of scrapie incubation period by an injection of dextran sulphate 500 within the month before or after infection. J Gen Virol. 67:463–473
73. Ladogana A, Casaccia P, Ingrosso L, Cibati M, Salvatore M, Xi Y et al (1992) Sulphate polyanions prolong the incubation period of scrapie-infected hamsters. J Gen Virol. 73:661–5. Available from: https://doi.org/10.1099/0022-1317-73-3-661

Publisher's note